Dynamics of biomembranes using level set and adaptive finite element methods

Aymen Laadhari, Pierre Saramito, Chaouqi Misbah

Dynamics of biomembranes using level set and adaptive finite element methods

Aymen Laadhari*+, Pierre Saramito* and Chaouqi Misbah+

Version 1.14 June 28, 2011

* Laboratoire Jean Kuntzmann, Université Joseph Fourier and CNRS, 51 rue des Mathématiques, B. P. 53, 38041 Grenoble Cedex 9, France.
+ Laboratoire Interdisciplinaire de Physique, 140 avenue de la physique, Université Joseph Fourier, and CNRS, 38402, Saint Martin d'Hères, France.

Abstract – *The numerical simulation of the deformation of vesicle membranes under simple shear external fluid flow is considered in this paper. A new saddle-point approach is proposed for the imposition if the fluid incompressibility and the membrane inextensibility constraints, through Lagrange multipliers defined in the fluid and on the membrane respectively. Using a level set formulation, the problem is approximated with mixed finite elements combined with an automatic adaptive mesh procedure at the vicinity of the membrane boundary. Numerical experiments show that this combination of the saddle-point and adaptive mesh method enhances the accuracy of the method.*

1 Introduction

Phospholipid membranes are abundant in biology. They represent the major component of the cytoplasmic membrane of real cells. They are also present within the cell cytoplasm, e.g. the Golgi apparatus, a complex assembly of phospholipid layers which serve to form small vesicles for protein transport. Phospholipid membranes are also used in many industrial applications, as in giant liposome emulsions for cosmetics. A simple closed membrane of pure phospholipid suspended in an aqueous solution, also called a suspension of *vesicles*, constitute an attractive model system in order to describe mechanical and viscoelastic behaviors of many cells, like red blood cells. They are also considered as promising drug carriers for a delivery at specific sites in the organisms. This explains the increasing interest for biological membranes from various communities ranging from biology [35, 31] to applied mathematics [33, 20, 4]. This contribution is concerned with a certain aspect of mathematical modeling of vesicles, and more generally of phospholipid membranes.

Vesicles are formed by amphiphilic molecules self-assembled in water to build bilayers, in a certain range of concentration and temperature. At room, as well as at the physiological temperature, the membrane is a two dimensional incompressible fluid. Due to incompressibility, the main mode of deformation of a vesicle is bending. A basic ingredient for biomembranes is thus bending energy. Canham [9] and Helfrich [36, 37] introduced the following expression of the bending energy:

$$\frac{k}{2}\int_\Gamma (H-H_0)^2\,\mathrm{d}s + \frac{k_g}{2}\int_\Gamma K\,\mathrm{d}s, \tag{1}$$

where $H = H_1 + H_2$ is the mean curvature of the membrane surface, with H_1 and H_2 are the principle curvatures and $K = H_1H_2$ is the Gauss curvature. The membrane surface is denoted by Γ while Ω represents the volume inside the vesicle, such that $\Gamma = \partial\Omega$. The integrals are performed along the membrane surface where $\mathrm{d}s$ denotes a surface area, while, in this paper, $\mathrm{d}x$ will represent a volume element. The constants k and k_g have the dimension of an energy and represent

the bending modulus and the Gaussian curvature modulus, respectively. Also H_0 denotes the spontaneous curvature that describes the asymmetry of the membrane. In this paper, $H_0 = 0$, since H_0 is relevant only for three-dimensional problems (see appendix A) and we restrict to the bidimensional case in this paper. Finally, from the Gauss-Bonnet theorem, the second term of the Canham-Helfrich energy (1) is a topological invariant. Since topological changes are not considered in this paper, this second term is omitted here.

Vesicles can be more or less inflated. The deflation could be due to osmotic effects, depending on additives in the solution. It could also be due to thermal effects: the thermal expansion of phospholipides is greater than those of the water inside the membrane, and thus, the area A_0 of the vesicle increases more rapidly than its volume V_0. The *reduced volume*, denoted as γ, measures the deflation:

$$\gamma = \frac{3V_0}{4\pi} \times \left(\frac{4\pi}{A_0}\right)^{3/2} \in]0, 1]. \tag{2}$$

Thus, γ compares the vesicle volume V_0 with the volume of a sphere having the area equal to A_0: γ is a number without dimension, that equals to 1 when the vesicle is a sphere and is lower than 1 otherwise. For instance, for the human red blood cell $\gamma \approx 0.64$. By varying γ, the shape that minimizes the energy of curvature can vary from an ellipsoid stretched to a biconcave shape, towards forms varied as that of the Peanut. In the two-dimensional case, V_0 and A_0 denotes the area and the perimeter respectively. The reduced area γ compares the area of the vesicle with the area of a circle having the same perimeter as the vesicle. The reduced area is expressed in the two-dimensional case by:

$$\gamma \quad = \quad \frac{V_0}{\pi} \times \left(\frac{2\pi}{A_0}\right)^2.$$

Notice that, for a circle, the reduced area equals to 1.

Notice that the vesicle membrane is impermeable (no osmosis), the number of molecules remains fixed in each layer, and the energetic cost of stretching or compressing the membrane is much larger than the cost of bending deformations: the membrane could be considered as inextensible. In order to satisfy this inextensibility constraint, two approaches are commonly available. The first one use the penalty approach, together with a penalty parameter (see e.g. [10, 12]): the inextensibility constraint then is not exactly satisfied and the approximate solution depends upon the penalty parameter. The second solution introduces a Lagrange multiplier, that interprets as the surface tension of the membrane, and the inextensibility constraints is exactly satisfied. In our present work, the second solution was selected, since it avoid the dependence of the solution upon the penalty parameter. Despite it has not yet retain attentions in the context of membrane vesicle application, it is of common use for incompressible fluid flow applications (see e.g. [32]).

Furthermore, for general interface fluid flow problems, there are two main classes of numerical methods usually used: the Lagrangian methods class based on an explicit interface parameterization and discretization while the Eulerian methods class uses an implicit function that expresses the interface by its equation. The popular phase field and level set methods fall into this second class.

For Lagrangian methods, the interface, which represents here the biological membrane, is discretized by a set of points which are going to be moved with a speed depending on the studied problem. The mesh, capturing the interface, may regenerated at each time step, while the boundary conditions between inside and outside volume of the interface could be directly imposed at the element level. The older

method used for vesicle fluid application falls into this category: the *boundary element method* transforms all viscous volume terms into surface integrals through a Green kernel and only a surface mesh of the interface is required [29, 30]. Nevertheless, inertia terms are not reducible to boundary integrals and, despite some recent improvements, this approach suffers from some limitations. A more recent approach bases on both a mesh of the interface and a volume mesh. When the volume mesh is compatible with the interface discretization, the *classical finite element method* could be used [8]. A commonly used variant fixes the volume mesh one time for all and expresses interface integrals on a discrete moving surface mesh: this is the so called *penalty immersed boundary method* [22, 23].

The Eulerian methods are characterized by the use of a meshing strategy that is independent of the movements of the interface: this approach allows the use of fixed and fully structured volume mesh. Moreover, no more surface mesh of the moving interface is required. Very complex shapes, with strong variations of the curvature and possible topological changes, becomes also possible. In the case of a diffuse interface, as for fluid mixtures, the interface is represented by a smooth transition zone. Indeed, at least at the molecular scale, there is a small zone of mixture between species. From a numerical point of view, the diffuse interface notion could be interpreted as a way of regularization of a sharp model interface, together with a regularization parameter, associated to the interface width: this is the *phase field method*, introduced by Allen and Cahn [2], and applied recently to vesicles [5, 11]. A second Eulerian method, the *level set method* [27], do no more requires any regularization and is able to catch sharp interfaces: a simple transport equation is used to move the level set function. See [26] for applications to vesicle dynamics.

Nevertheless, both phase field and level set methods suffer a lack of precision when dealing with the inextensibility constraints. In this paper we develop a new level set method that exactly solve these constraints at the discrete level: it extends to the vesicle dynamics a previous work on level set methods for the advection equation [25].

In the present work we focus our attention on describing the dynamics of a single suspended vesicle in a linear shear gradient of a plane flow. Vesicles in shear flow in the limit of the vanishing Reynolds number (also called the Stokes limit) have been the subject of extensive studies [4]. In the present work, inertia terms are not neglected, and non-zero Reynolds numbers are considered. This situation is more realistic for both red blood cells and vesicle practical flows applications.

An outline of the paper is as follows. A saddle-point approach allows us to characterize the solution in a weak formulation, which is discretized using mixed finite elements in section 2. In Section 3 we focus on the numerical method. We present our level set method formulation for the vesicle dynamics and show the finite element discretization as well the advection mass preservation improvement. Section 4 is devoted to show numerical results illustrating the vesicle membrane in the tumbling and the tank-treading regimes. Finally, for the first time, the effect of the inertia terms is elaborated and we show that beyond a critical value of the number of Reynolds the vesicle passes from a tumbling to a tank-treading regime.

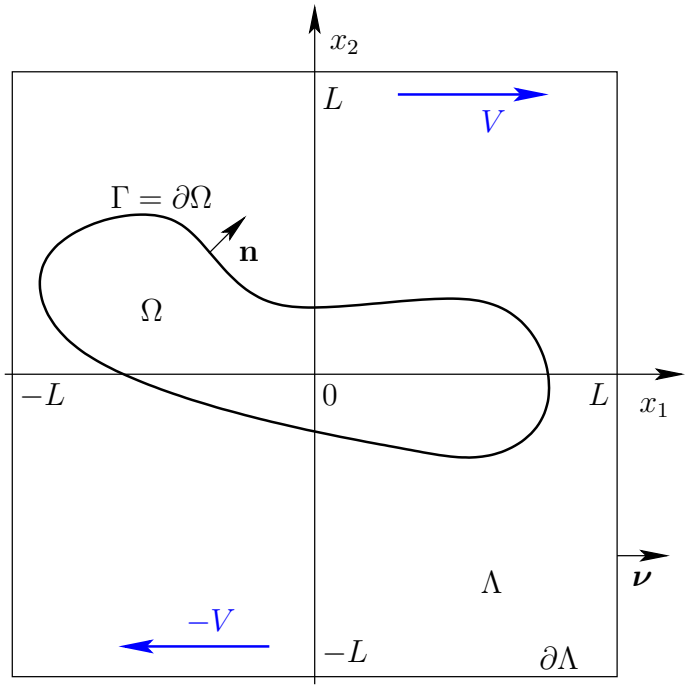

Figure 1: Notations for the vesicle interacting with a surrounding shear flow.

2 Problem statement

2.1 Notations and preliminary results

Let $\Lambda =]-L, L[^d$ be the bounded region containing the vesicle and the surrounding fluid. Numerical computations are performed in this paper with $d = 2$ while the mathematical formulation is also valid when $d = 3$. Let $T > 0$: for any $t \in]0, T[$, the membrane $\Gamma(t) \subset \Lambda$ is the closed surface defined by:

$$\Gamma(t) = \{(t, x) \in]0, T[\times\Lambda; \quad \phi(t, x) = 0\}, \tag{3}$$

where ϕ is the level set function. By convention, the vesicle $\Omega(t) \subset \Lambda$ is the region where $\phi(t, .)$ is negative and we have $\Gamma(t) = \partial\Omega(t)$.

Let $\mathbf{u}$ denotes the velocity of the fluid in Λ. The membrane $\Gamma(t)$ is transported at the same velocity, and thus, the level set function satisfies:

$$\frac{D\phi}{Dt} = \frac{\partial\phi}{\partial t} + \mathbf{u}.\nabla\phi = 0 \quad \text{in} \quad]0, T[\times\Lambda, \tag{4a}$$

where $D\phi/Dt$ denotes the material derivative. The previous transport equation may be completed by suitable boundary and initial conditions:

$$\phi = \phi_b \quad \text{on} \quad]0, T[\times\Sigma_- \tag{4b}$$

$$\phi(0) = \phi_0 \quad \text{in} \quad \Lambda \tag{4c}$$

where $\Sigma_- = \{x \in \partial\Lambda; \ \mathbf{u}.\boldsymbol{\nu}(x) < 0\}$ is the upstream and $\boldsymbol{\nu}$ denotes the outward unit normal to the surrounding bounding box Λ. Concerning the initial condition (4c), the function ϕ_0 denotes the *signed distance* between x and the given initial shape

membrane $\Gamma(0)$:

$$\phi_0(x) = \begin{cases} \inf\{|y-x|;\ y\in\Gamma(0)\} & \text{when } x\notin\Omega(0), \\ \inf\{-|y-x|;\ y\in\Gamma(0)\} & \text{otherwise.} \end{cases}$$

Let $\mathbf{n}$ denotes the unit outward normal vector to the shape Ω (see Fig. 1). Let f be any scalar function and $\mathbf{v}$ be any vector field. The surface gradient, the surface divergence and the Laplace-Beltrami operator are respectively expressed by:

$$\nabla_s f = (I-\mathbf{n}\otimes\mathbf{n})\,\nabla f = \nabla f - (\mathbf{n}.\nabla f)\,\mathbf{n}, \tag{5a}$$

$$\mathrm{div}_s\,\mathbf{v} = (I-\mathbf{n}\otimes\mathbf{n}) : \nabla\mathbf{v} = \mathrm{div}\,\mathbf{v} - ((\nabla\mathbf{v}).\mathbf{n}).\mathbf{n}, \tag{5b}$$

$$\Delta_s f = \mathrm{div}_s\,(\nabla_s f)\,. \tag{5c}$$

Here, $\otimes$ denotes the tensorial product of two vectors and the semicolumn : is the two times contracted product between tensors.

The mean and the Gauss curvatures can be expressed in terms of the normal $\mathbf{n}$ (see [24]):

$$H = \nabla_s.\mathbf{n} = \nabla.\mathbf{n},$$
$$2K = H^2 - \nabla\mathbf{n} : \nabla\mathbf{n}^T.$$

2.2 Minimization and saddle-point formulations

For any velocity field $\mathbf{u}$ defined in Λ, the instantaneous energy of the system is defined at any time $t\in]0,T[$ by:

$$J(\mathbf{u}) = \frac{\mathrm{d}}{\mathrm{d}t}\left(\int_\Lambda \frac{\rho}{2}\,|\mathbf{u}|^2\,\mathrm{d}x\right) + \int_\Lambda \eta\,|D(\mathbf{u})|^2\,\mathrm{d}x + \int_{\Gamma(t)} \frac{k}{2}H^2\,\mathrm{d}s. \tag{6}$$

where $D(\mathbf{u}) = (\nabla\mathbf{u} + (\nabla\mathbf{u})^T)/2$ is the symmetric part of the gradient of velocity tensor and $|.|$ denotes the Euclidean norms of vectors or tensors. The previous expression of the energy includes three terms, from left to right: the kinetic energy, the viscous energy and the Canham-Helfrich bending energy. There are three corresponding scalar parameters: ρ is the density, supposed constant, η is the viscosity and k the bending modulus of the Canham-Helfrich energy introduced in (1). In practice, the viscosity η is not constant over Λ: it takes a constant value η_0 outside the vesicle $\Omega(t)$ and a different constant value inside the vesicle.

Notice that, in the bending energy term in (6), the membrane $\Gamma(t)$ depends upon the velocity field $\mathbf{u}$ via (3) and the level-set function ϕ, satisfying the transport problem (4) that involves $\mathbf{u}$. Also, the curvature H on $\Gamma(t)$ depends implicitly upon $\mathbf{u}$.

The unknown velocity field may satisfy the boundary conditions and two additional constraints: the fluid mass conservation and the membrane inextensibility. The mass conservation reduces to the divergence-free condition $\mathrm{div}\,\mathbf{u}=0$ since the density ρ is constant. Conversely, the membrane inextensibility writes locally $\mathrm{div}_s\,\mathbf{u}=0$. Let us introduce the following spaces of admissible velocities:

$$\mathbb{V}(\mathbf{u}_b) = \left\{\mathbf{v}\in\left(H^1(\Lambda)\right)^d;\ \mathbf{v}=\mathbf{u}_b \ \text{ on } \Sigma_D\right\},$$
$$\mathbb{K}(t,\mathbf{u}_b) = \left\{\mathbf{v}\in\mathbb{V}(\mathbf{u}_b);\ \mathrm{div}\,\mathbf{v}=0 \text{ in } \Lambda \text{ and } \mathrm{div}_s\,\mathbf{v}=0 \text{ on } \Gamma(t)\right\}.$$

The boundary $\Sigma_D =]-L,L[^{d-1}\times\{-L,L\}$ is associated to the Dirichlet boundary condition $\mathbf{u}_b(t,x)$, expressed for a shear flow by:

$$\mathbf{u}_b(t,x) = \begin{cases} V & \text{when } x_d = L \\ -V & \text{when } x_d = -L \end{cases}$$

for all $(t,x) \in]0,T[\times\Sigma_D$. Here, V denotes the given shear velocity at the surrounding box boundary (see Fig. 1). Finally, the problem expresses as a minimization one:

find $\mathbf{u} \in C^0\left(]0,T[, L^2(\Lambda)^d\right) \cap L^2\left(]0,T[, \mathbb{K}(t,\mathbf{u}_b)\right)$ *such that*

$$\left\{\begin{array}{rcl} \mathbf{u}(t) & = & \underset{\mathbf{v}\in\mathbb{K}(t,\mathbf{u}_b)}{\arg\inf}\ J(\mathbf{v}),\ \forall t \in]0,T[, \\ \\ \mathbf{u}(0) & = & \mathbf{u}_0 \ \text{ in } \ \Lambda. \end{array}\right.$$

where $\mathbf{u}_0$ is the given initial velocity. This is a strongly nonlinear shape optimization problem, expressed in terms of the unknown $\mathbf{u}$.

The space of admissible velocities $\mathbb{K}(t,\mathbf{u}_b)$ contains the incompressibility and inextensibility constraints: it is not suitable for practical finite element discretization, since there are no known finite element basis of such spaces. Conversely, the unconstrained space of $\mathbb{V}(\mathbf{u}_b)$ is of practical interest: the two constraints can be imposed via two Lagrange multipliers: the pressure p and the surface tension λ. Let us introduce the following Lagrangian:

$$\mathscr{L}(\mathbf{u};\, p, \lambda) = J(\mathbf{u}) + \int_\Lambda p \operatorname{div} \mathbf{u}\, \mathrm{d}x + \int_{\Gamma(t)} \lambda \operatorname{div}_s \mathbf{v}\, \mathrm{d}s.$$

The previous minimization problem can be rewritten as a saddle point problem:

find $\mathbf{u} \in C^0\left(]0,T[, L^2(\Lambda)^d\right) \cap L^2\left(]0,T[, \mathbb{V}(\mathbf{u}_b)\right)$, $p \in L^2\left(]0,T[, L^2(\Lambda)\right)$
and $\lambda \in L^2\left(]0,T[, H^{\frac{1}{2}}(\Lambda)\right)$ *such that*

$$\left\{\begin{array}{rcl} (\mathbf{u},p,\lambda) & = & \underset{\mathbf{v}\in\mathbb{V}(\mathbf{u}_b)}{\arg\inf} \ \underset{\substack{q\in L^2(\Lambda) \\ \mu\in H^{\frac{1}{2}}(\Gamma(t))}}{\sup} \ \mathscr{L}(\mathbf{v};\, q, \mu), \\ \\ \mathbf{u}(0) & = & \mathbf{u}_0 \ \text{ in } \ \Lambda. \end{array}\right.$$

Here $H^{\frac{1}{2}}(\Gamma)$ denotes as usual [1] the space of the trace of elements of $H^1(\Omega)$ on Γ.

2.3 Variational formulation

Since the Lagrangian $\mathscr{L}$ is differentiable, the saddle point $(\mathbf{u};p,\lambda)$ satisfies the following variational optimality equations:

$$\begin{array}{rcll} \dfrac{\partial \mathscr{L}}{\partial \mathbf{u}}(\mathbf{u};\, p,\lambda)(\mathbf{v}) & = & 0, & \forall \mathbf{v} \in \mathbb{V}(0), \\ \dfrac{\partial \mathscr{L}}{\partial p}(\mathbf{u};\, p,\lambda)(q) & = & 0, & \forall q \in L^2(\Lambda), \\ \dfrac{\partial \mathscr{L}}{\partial \lambda}(\mathbf{u};\, p,\lambda)(\mu) & = & 0, & \forall \mu \in H^{\frac{1}{2}}(\Gamma)\,. \end{array}$$

After expansion of the derivatives of $\mathscr{L}$, the optimality conditions leads to the following variational formulation of the problem:

find $\mathbf{u} \in C^0\left(]0,T[, L^2(\Lambda)^d\right) \cap L^2\left(]0,T[, \mathbb{V}(\mathbf{u}_b)\right)$, $p \in L^2\left(]0,T[, L^2_0(\Omega)\right)$

and $\lambda \in L^2\left(]0,T[, H^{\frac{1}{2}}(\Gamma)\right)$ *such that*

$$\begin{aligned}
\int_\Lambda \rho \frac{D\mathbf{u}}{Dt}.\mathbf{v}\,\mathrm{d}x + \int_\Lambda 2\eta\, D(\mathbf{u}) : D(\mathbf{v})\,\mathrm{d}x & \\
+ \int_\Lambda p\ \mathrm{div}\,\mathbf{v}\,\mathrm{d}x + \int_{\Gamma(t)} \lambda\, \mathrm{div}_s\,\mathbf{v}\,\mathrm{d}s &= \int_{\Gamma(t)} \mathbf{f}.\mathbf{v}\,\mathrm{d}s, \quad \forall \mathbf{v} \in \mathbb{V}(0), \qquad (7a)\\
\int_\Lambda q\ \mathrm{div}\,\mathbf{u}\,\mathrm{d}x &= 0, \quad \forall q \in L^2(\Lambda), \qquad (7b)\\
\int_{\Gamma(t)} \mu\, \mathrm{div}_s\,.\mathbf{u}\,\mathrm{d}s &= 0, \quad \forall \mu \in H^{\frac{1}{2}}(\Gamma(t)). \qquad (7c)
\end{aligned}$$

together with the initial condition $\mathbf{u}(0) = \mathbf{u}_0$. Recall that $\Gamma(t)$ is given by (3) in terms of the level set function ϕ, which is solution of the transport problem (4a)-(4c) involving $\mathbf{u}$. Also, $\dfrac{D\mathbf{u}}{Dt} = \partial_t\mathbf{u} + \mathbf{u}.\nabla\mathbf{u}$ denotes the nonlinear inertia term. The strength $\mathbf{f}$, that appears in the right-hand-side of (7a), is associated to the Canham-Helfrich bending energy and is given by [24]:

$$\mathbf{f} = k\left\{\Delta_s H + H\left(\frac{H^2}{2} - 2K\right)\right\}\mathbf{n}.$$

This is not an obvious computation, since $\Gamma(t)$ and H depend implicitly upon $\mathbf{u}$: it requires some advanced shape optimization tools. In the two-dimensional case, since $K = 0$, this expression reduces to: $\mathbf{f} = k\left(\Delta_s H + H^3/2\right)\mathbf{n}$. Remark that, since J is not convex in general, the optimality system (7) could include both local minimums and maximums of the energy J. Thus, the optimality system is not equivalent to the minimization or saddle-point problems ; nevertheless, a minimum of J is also a solution of the optimality system.

2.4 Strong formulation

In order to deal with the integrals over $\Gamma(t)$, a generalization of the Green formulæ over the closed surface $\Gamma(t)$ is used (see e.g. [24]):

$$\int_\Gamma \nabla_s\mu.\mathbf{v}\,\mathrm{d}s + \int_\Gamma \mu\,\mathrm{div}_s\,\mathbf{v}\,\mathrm{d}s = \int_\Gamma \mu\,\mathbf{v}.\mathbf{n}\,H\,\mathrm{d}s, \quad \forall \mu \in H^{\frac{1}{2}}(\Gamma), \quad \forall \mathbf{v} \in H^1(\Lambda). \qquad (8)$$

Equation (7a) is then integrated by parts on Ω and $\Lambda\backslash\Omega$ and terms are then merged. Thus, for all $\mathbf{v} \in \mathbb{V}(0)$, we have:

$$\begin{aligned}
\int_\Lambda \rho \frac{D\mathbf{u}}{Dt}.\mathbf{v}\,\mathrm{d}x - \int_\Lambda \mathbf{div}\left(2\eta\, D(\mathbf{u}) - pI\right).\mathbf{v}\,\mathrm{d}x + \int_{\partial\Lambda} \left\{\left(2\eta\, D(\mathbf{u}) - pI\right).\boldsymbol{\nu}\right\}.\mathbf{v}\,\mathrm{d}s & \\
+ \int_{\Gamma(t)} \left\{\left[2\eta\, D(\mathbf{u}) - pI\right].\mathbf{n}\right\}.\mathbf{v}\,\mathrm{d}s - \int_{\Gamma(t)} \nabla_s\lambda.\mathbf{v}\,\mathrm{d}s + \int_{\Gamma(t)} \lambda\, H\mathbf{n}.\mathbf{v}\ \mathrm{d}s & \\
= \int_{\Gamma(t)} \mathbf{f}.\mathbf{v}\,\mathrm{d}s &
\end{aligned}$$

where [.] denotes the jump of a quantity across $\Gamma(t)$ in the direction $\mathbf{n}$ of the normal, I is the identity tensor and **div** is the divergence of a symmetric tensor, defined as the divergence of its row or column vectors.

Finally, the strong form of the problem writes:

find ϕ, $\mathbf{u}$, p *and* λ *such that*

$$\frac{\partial \phi}{\partial t} + \mathbf{u}.\nabla\phi = 0 \text{ in }]0,T[\times\Lambda \tag{9a}$$

$$\rho\left(\frac{\partial \mathbf{u}}{\partial t} + \mathbf{u}.\nabla\mathbf{u}\right) - \mathbf{div}\left(2\eta\, D(\mathbf{u})\right) + \nabla p = 0 \text{ in }]0,T[\times(\Lambda\backslash\Gamma) \tag{9b}$$

$$\operatorname{div}\mathbf{u} = 0 \text{ in }]0,T[\times\Lambda \tag{9c}$$

$$[\mathbf{u}] = 0 \text{ on }]0,T[\times\Gamma \tag{9d}$$

$$-k\left\{\Delta_s H + H\left(\frac{H^2}{2} - 2K\right)\right\}\mathbf{n} + H\,\lambda\,\mathbf{n} - \nabla_s\lambda + \left[2\eta\, D(\mathbf{u}) - pI\right].\mathbf{n} = 0 \text{ on }]0,T[\times\Gamma \tag{9e}$$

$$\operatorname{div}_s\mathbf{u} = 0 \text{ on }]0,T[\times\Gamma \tag{9f}$$

$$\phi = \phi_b \text{ on }]0,T[\times\Sigma_- \tag{9g}$$

$$\mathbf{u} = \mathbf{u}_b \text{ on }]0,T[\times\Sigma_D \tag{9h}$$

$$(2\eta D(\mathbf{u}) - pI).\boldsymbol{\nu} = 0 \text{ on }]0,T[\times\Sigma_N \tag{9i}$$

$$\phi(0) = \phi_0 \text{ in } \Lambda \tag{9j}$$

$$\mathbf{u}(0) = \mathbf{u}_0 \text{ in } \Lambda \tag{9k}$$

where $\Sigma_N = \{-L, L\}^{d-1}\times]-L, L[$ is associated to a Neumann-type boundary condition.

Notice that equation (9b) is written in $\Lambda\backslash\Gamma$, i.e. in Ω and its complementary $\Lambda\backslash\overline{\Omega}$. On Γ, the jump term in (9e) points out the balance with membrane strengths: indeed, the first normal term comes from the Canham-Helfrich bending energy. This energy being a purely geometrical quantity, it cannot give rise to a tangential strength: any tangential movement of points on a surface is only modifying their positions without affecting the shape of the surface and its curvature energy. The second and third terms in (9e) involves the Lagrange multiplier λ, known as the surface tension, and defined on the membrane $\Gamma(t)$. The second term is normal and it is similar to the strengths of capillarities engendered by the surface tension when modelling of the dynamics of drops. The term term $\nabla_s\lambda$ is tangential and its action is known as the Marangoni effect.

2.5 Dimensionless problem

Let us put the problem in dimensionless form. The characteristic length R_0 of the vesicle is chosen equal to the radius of a sphere having the same surface as the vesicle Γ in the tree dimensional case. In the two-dimensional case, it represents the radius of a circle having the same perimeter as Γ. The characteristic velocity $U = VR_0/L$ is chosen to be equal to the shear velocity at a distance R_0 from the center. The characteristic viscosity η_0 is chosen as the viscosity of the fluid at the exterior of the membrane.

Let us introduce the following four dimensionless numbers:

$$Re = \frac{\rho R_0 U}{\eta_0}, \quad Ca = \frac{\eta_0 R_0^2 U}{k}, \quad \alpha = \frac{R_0}{L} \text{ and } \beta = \frac{\eta_1}{\eta_0}$$

The Reynolds number Re, as usual, expresses the ratio of inertia effects with the viscous ones. The capillarity number Ca compares the strength of the imposed flow $\eta_0 U/R_0$ to the bending resistance of the membrane k/R_0^3. The dimensionless number α represents the confinement of the vesicle in the shear flow and β is the

viscosity ratio. The initial shape $\Gamma(0)$ is also characterized by a five-th dimensionless number γ, the reduced area, already introduced in (2).

In the rest of the paper, only dimensionless quantities are used and, since there is no ambiguity, there are still denoted with the same notations as the original quantities. The dimensionless boundary condition writes:

$$\mathbf{u}_b(t,x) = \left\{ \begin{array}{ll} 1/\alpha & \text{when } x_d = \alpha \\ -1/\alpha & \text{when } x_d = -\alpha \end{array} \right.$$

A dimensionless viscosity function is also defined:

$$\eta_*(t,x) = \left\{ \begin{array}{ll} \beta & \text{when } x \in \Omega(t) \\ 1 & \text{otherwise} \end{array} \right.$$

The dimensionless problem writes:

find ϕ, $\mathbf{u}$, p and λ such that

$$\begin{aligned}
\frac{\partial \phi}{\partial t} + \mathbf{u}.\nabla\phi &= 0 \quad \text{in }]0,T[\times\Lambda && \text{(10a)}\\
Re\left(\frac{\partial \mathbf{u}}{\partial t} + \mathbf{u}.\nabla\mathbf{u}\right) - \mathbf{div}\left(2\eta_*\, D(\mathbf{u})\right) + \nabla p &= 0 \quad \text{in }]0,T[\times(\Lambda\backslash\Gamma) && \text{(10b)}\\
\operatorname{div}\mathbf{u} &= 0 \quad \text{in }]0,T[\times\Lambda && \text{(10c)}\\
[\mathbf{u}] &= 0 \quad \text{on }]0,T[\times\Gamma && \text{(10d)}\\
-\frac{1}{Ca}\left\{\Delta_s H + H\left(\frac{H^2}{2} - 2K\right)\right\}\mathbf{n} & \\
+H\,\lambda\,\mathbf{n} - \nabla_s\lambda + \left[2\eta_*\, D(\mathbf{u}) - pI\right].\mathbf{n} &= 0 \quad \text{on }]0,T[\times\Gamma && \text{(10e)}\\
\operatorname{div}_s \mathbf{u} &= 0 \quad \text{on }]0,T[\times\Gamma && \text{(10f)}\\
\phi &= \phi_b \quad \text{on }]0,T[\times\Sigma_- && \text{(10g)}\\
\mathbf{u} &= \mathbf{u}_b \quad \text{on }]0,T[\times\Sigma_D && \text{(10h)}\\
(2\eta D(\mathbf{u}) - pI).\boldsymbol{\nu} &= 0 \quad \text{on }]0,T[\times\Sigma_N && \text{(10i)}\\
\phi(0) &= \phi_0 \quad \text{in } \Lambda && \text{(10j)}\\
\mathbf{u}(0) &= \mathbf{u}_0 \quad \text{in } \Lambda && \text{(10k)}
\end{aligned}$$

where the normal and the curvature are expressed in term of the level set function: $\mathbf{n} = \nabla\phi/|\nabla\phi|$ and $H = div_s\,\mathbf{n}$. Biophysical applications, as the prediction of vesicles behavior in small blood vessels, is our aim in this paper, and constitute a guideline for the choice of dimensionless parameters. Following Vitkova and al. [34] on vesicles under shear flow, we estimate the physical parameters:

$$\begin{array}{lllllll}
R_0 & \approx & 5\times10^{-5} & \text{m}, & \rho & \approx & 10^3 \quad \text{kg/m}^3,\\
L & \approx & 10^{-3} & \text{m}, & \eta_0 & \in & \left[5\times10^{-4},\ 0.2\right] \quad kg.s^{-1}.m^{-1},\\
k & \approx & 10^{-19} & \text{J}. & & &
\end{array}$$

The shear velocity at the wall V is between 1.2×10^{-2} and 0.12 m/s while the vesicles are deflated with γ between 0.92 and 0.99. These experimental values leads to consider the following dimensionless parameter ranges:

$$\begin{array}{lll}
Re & \in & \left[1.5\times10^{-9},\ 1.5\times10^{-4}\right],\\
Ca & \in & \left[3\times10^{3},\ 3\times10^{6}\right].
\end{array}$$

While the experimental value of the confinement was $\alpha = 1/20$, the influence of this parameter is studied by varying its value between $1/2$ and $1/5$ in the case of regular

meshes and reaching 1/12 when using adaptive meshes methods, as presented in the next section. Finally, the viscosity ratio β is varying around a critical value associated to a stability transition and are less than 20.

3 Numerical methods

3.1 Time discretization and the characteristic method

For simplicity, the numerical methods are presented when $d = 2$: in that case the Gauss curvature is null: $K = 0$. Nevertheless, the methods extend to three-dimensional case, just inserting the computation of K in the Canham-Helfrich force.

Let $0 = t^0 < t^1 < t^2 < ... < t^N = T$ be a subdivision of the time interval $[0, T]$ with a constant time step $\Delta t = t^{n+1} - t^n$, $n = 1, 2, ..., N$. At step $n = 0$, let $\phi^0 = \phi_0$ be the initial condition. For any $n \geq 1$, the unknowns ϕ^n, $\mathbf{u}^n$, p^n and λ^n at time step n are computed by induction, using values at previous time steps. The time discretization is performed by using the method of characteristics: for any $t > 0$ and $x \in \Lambda$, the characteristic curve $X(., x, ; t)$ passing at time t through x is defined by the following ordinary differential equation:

$$\left\{ \begin{array}{rcl} \dfrac{\partial X}{\partial t}(s, x; t) & = & \mathbf{u}\left(X(s, x; t), t\right), \quad s \in]0, T[\\ X(t, x; t) & = & x. \end{array} \right.$$

For any function $\varphi(t, x)$, the total derivative $D\varphi/Dt$ expresses:

$$\frac{D\varphi}{Dt}(t, x) = \left(\frac{\partial \varphi}{\partial t} + \mathbf{u}.\nabla\varphi\right)(t, x) = \frac{\partial}{\partial \tau}\left(\varphi\left(X(t, x; \tau), \tau\right)\right)|_{\tau=t}$$

Following Pironneau [28], this derivative is approximated by a first-order backward Euler scheme:

$$\frac{D\varphi}{Dt}(t^n, x) \approx \frac{\varphi(t^n, x) - \varphi(t^{n-1}, X_1^{n-1}(x))}{\Delta t}$$

where $X_1^{n-1}(x) = x - \Delta t\ \mathbf{u}^{n-1}(x)$ denotes the first-order forward Euler approximation of $X(t^{n-1}, x; t^n)$.

$$\phi^n = \phi^{n-1} \circ X_1^{n-1} \quad \text{in } \Lambda \tag{11}$$

Then, the vesicle shape at step n is known:

$$\begin{array}{rcl} \Gamma^n & = & \{x \in \Lambda;\ \phi^n(x) = 0\} \\ \Omega^n & = & \{x \in \Lambda;\ \phi^n(x) < 0\} \end{array}$$

The dimensionless viscosity is also computed explicitly:

$$\eta_*^n = \left\{ \begin{array}{ll} \beta & \text{when } x \in \Omega^n \\ 1 & \text{otherwise} \end{array} \right.$$

Also, the normal $\mathbf{n}^n$ and the curvatures H^n and K^n are computed at this step, together with differential operators (5) on the surface Γ^n, and defined for any scalar function f and any vector field $\mathbf{v}$ by:

$$\nabla_s^n f = (I - \mathbf{n}^n \otimes \mathbf{n}^n)\ \nabla f, \tag{12a}$$

$$\mathrm{div}_s^n\, \mathbf{v} = (I - \mathbf{n}^n \otimes \mathbf{n}^n) : \nabla \mathbf{v}, \tag{12b}$$

$$\Delta_s^n f = \mathrm{div}_s^n\ (\nabla_s^n f)\,. \tag{12c}$$

For any $y \in \mathcal{C}^3([0,T])$, a Taylor expansion shows that:

$$\frac{\mathrm{d}y}{\mathrm{d}t}(t) = \frac{3y(t) - 4y(t-\Delta t) + y(t-2\Delta t)}{2\Delta t} + \mathcal{O}\left(\Delta t^2\right).$$

Based on this approximation and following [32, chap. 5], the time discretization of the inertia term is performed using a second order combined characteristic and finite difference discretization method. Let us introduce the second-order characteristics:

$$\begin{aligned} \mathbf{u}^* &= 2\mathbf{u}^{n-1} - \mathbf{u}^{n-2} \\ X_2^{n-1}(x) &= x - \Delta t\ \mathbf{u}^*(x) \quad \text{a.e. } x \in \Lambda, \\ X_2^{n-2}(x) &= x - 2\Delta t\ \mathbf{u}^*(x) \quad \text{a.e. } x \in \Lambda. \end{aligned}$$

Notice that $\mathbf{u}^*$ represents a prediction by extrapolation of $\mathbf{u}$ at time t_n. The problem becomes:

find $\mathbf{u}^n$, p^n *and* λ^n *such that*

$$\begin{aligned} &\frac{Re}{2\Delta t}\left(3\mathbf{u}^n - 4\mathbf{u}^{n-1} o X_2^{n-1} + \mathbf{u}^{n-2} o X_2^{n-2}\right) \\ &\qquad -\mathbf{div}\left(2\eta_*^n D\left(\mathbf{u}^n\right)\right) + \nabla p^n = 0 \quad \text{in } \Lambda\backslash\Gamma^n, \quad (13a) \\ &\qquad \operatorname{div}\mathbf{u}^n = 0 \quad \text{in } \Lambda, \quad (13b) \\ &\qquad [\mathbf{u}^n] = 0 \quad \text{on } \Gamma^n, \quad (13c) \\ &\qquad -\frac{1}{Ca}\left(\Delta_s^n H^n + \frac{\left(H^n\right)^3}{2}\right)\mathbf{n}^n \\ &\qquad +H^n\lambda^n\mathbf{n}^n - \nabla_s^n\lambda^n \\ &\qquad +\left[2\eta_*^n D\left(\mathbf{u}^n\right) - p^n\mathbf{I}\right].\mathbf{n}^n = 0 \quad \text{on } \Gamma^n, \quad (13d) \\ &\qquad \operatorname{div}_s^n.\mathbf{u}^n = 0 \quad \text{on } \Gamma^n, \quad (13e) \\ &\qquad \mathbf{u}^n = \mathbf{u}_b \quad \text{on } \Sigma_D. \quad (13f) \end{aligned}$$

The second order induction on $(\mathbf{u}^n)_{n\geq 0}$ is bootstrapped by using the initial condition: $\mathbf{u}^{-1} = \mathbf{u}^0 = \mathbf{u}_0$, where $\mathbf{u}^{-1}$ stands here for a convenient notation. The previous scheme use two main steps. The first step (11) is an explicit computation involving the characteristics. The second step (13) is a linear generalized Stokes sub-system that involves a constraint on the boundary of the vesicle together with the usual incompressibility constraint. We point out that this scheme transforms a strongly nonlinear shape optimization problem into a succession explicit computations and linear subproblems. The next paragraph presents how such a linear subproblem is treated.

3.2 The generalized Stokes subproblem

3.2.1 Formulation

Let us introduce the Canham-Helfrich force, that appears in the right-hand side of the generalized Stokes subproblem:

$$\mathbf{f}^n = \frac{1}{Ca}\left(\Delta_s^n H^n + \frac{\left(H^n\right)^3}{2}\right)\mathbf{n}^n. \quad (14)$$

where $\mathbf{n}^n = \nabla\phi^n/|\nabla\phi^n|$, $H^n = div_s\,\mathbf{n}^n$ and ϕ^n is supposed to be known at this step of the algorithm. The following bilinear forms are first introduced:

$$\begin{aligned} m(\mathbf{u},\mathbf{v}) &= \int_\Lambda \mathbf{u}.\mathbf{v}\,\mathrm{d}x,\ \forall \mathbf{u},\mathbf{v} \in \left(L^2(\Lambda)\right)^2, \\ a^n(\mathbf{u},\mathbf{v}) &= \int_\Lambda 2\,\eta_*^n\, D(\mathbf{u}) : D(\mathbf{v})\,\mathrm{d}x,\ \forall \mathbf{u},\mathbf{v} \in \left(H^1(\Lambda)\right)^2, \\ b_1(\mathbf{v},q) &= -\int_\Lambda q\,\mathrm{div}\,\mathbf{v}\,\mathrm{d}x,\ \forall q \in L^2(\Lambda),\ \forall \mathbf{v} \in H(\mathrm{div},\Lambda), \\ b_2^n(\mathbf{v},\mu) &= -\int_{\Gamma^n} \mu\,\mathrm{div}_s^n\,\mathbf{v}\,\mathrm{d}s,\ \forall \mu \in H^{\frac{1}{2}}(\Gamma^n),\ \forall \mathbf{v} \in H(\mathrm{div}_s,\Gamma^n). \end{aligned}$$

where $H(\mathrm{div},\Lambda) = \left\{\mathbf{s} \in \left(L^2(\Lambda)\right)^2;\ \mathrm{div}\,\mathbf{s} \in L^2(\Lambda)\right\}$ (see e.g. [15, 7]). The variational formulation of (13a)-(13f) writes:

(S): *find* $\mathbf{u}^n \in \mathbb{V}(\mathbf{u}_b)$, $p^n \in L^2(\Lambda)$ *and* $\lambda^n \in H^{\frac{1}{2}}(\Gamma^n)$ *such that*

$$\begin{aligned} &\frac{3Re}{2\Delta t} m\left(\mathbf{u}^n,\mathbf{v}\right) + a^n\left(\mathbf{u}^n,\mathbf{v}\right) + b_1\left(\mathbf{v},p^n\right) + b_2^n\left(\mathbf{v},\lambda^n\right) \\ &= m_s^n\left(\mathbf{f}^n,\mathbf{v}\right) + \frac{Re}{2\,\Delta t} m\left(4\mathbf{u}^{n-1}oX_2^{n-1} - \mathbf{u}^{n-2}oX_2^{n-2},\mathbf{v}\right), \qquad (15a) \\ &b_1\left(\mathbf{u}^n,q\right) = 0, \qquad (15b) \\ &b_2^n\left(\mathbf{u}^n,\mu\right) = 0, \qquad (15c) \end{aligned}$$

for all $\mathbf{v} \in \mathbb{V}(0)$, $q \in L^2(\Lambda)$ and $\mu \in H^{\frac{1}{2}}(\Gamma^n)$.

3.2.2 The Canham-Helfrich force

Let us consider in details the Canham-Helfrich force, as defined in (14). The force involves fourth order derivatives of the level set function and a direct discretization approach would requires a high regularity finite element method, such as the Hermite one (see e.g. [6]) with H^2 and C^1 regularity. In order to use standard Lagrange finite element, with only H^1 and C^0 regularity, the fourth-order derivatives are treated here with a different approach, based on a duality argument.

Since $H^n = \mathrm{div}\,\mathbf{n}^n$ and $\mathbf{n}^n = \nabla\phi^n/|\nabla\phi^n|$, then H^n expresses as a second order derivative of the level set function. Thus, a similar duality argument is then used. Let us define the *skeleton* of Ω as the set of points that are equidistant to at least two distinct points of $\partial\Omega$ (see e.g. [3, p. 195]). In order to avoid division by $|\nabla\phi^n|$, that could vanish on the skeleton, two intermediate variables $\mathbf{r}^n = \nabla(|\nabla\phi^n|)$ and $G^n = H^n|\nabla\phi^n|$ are used. First, using a classical Green formula in Λ, $\mathbf{r}^n$ can be characterized as

$$\mathbf{r}^n \in H_0(\mathrm{div},\Lambda) \text{ and } \int_\Lambda \mathbf{r}^n.\mathbf{s}\,\mathrm{d}x = \int_\Lambda |\nabla\phi^n|\ \mathrm{div}\,\mathbf{s}\ \mathrm{d}x, \quad \forall \mathbf{s} \in H_0(\mathrm{div},\Lambda),$$

where $H_0(\mathrm{div},\Lambda) = \{\mathbf{s} \in H(\mathrm{div},\Lambda);\ \mathbf{s}.\boldsymbol{\nu} = 0\}$. Next, let us turn to G^n. A simple development leads to:

$$G^n|\nabla\phi^n| = -H^n\ |\nabla\phi^n|^2 = -\mathrm{div}\left(\frac{\nabla\phi^n}{|\nabla\phi^n|}\right)|\nabla\phi^n|^2 = \mathbf{r}^n.\nabla\phi^n - \Delta\phi^n|\nabla\phi^n|$$

The duality argument is used for the $\Delta\phi^n$ term at the right-hand side and G^n is characterized by

$$G^n \in H^1(\Lambda) \text{ and } \int_\Lambda G^n\,\zeta\,|\nabla\phi^n|\,\mathrm{d}x = \int_\Lambda (\mathbf{r}^n.\nabla\phi^n)\,\zeta\,\mathrm{d}x + \int_\Lambda \nabla\phi^n.\nabla\zeta\,|\nabla\phi^n|\,\mathrm{d}x,\ \forall\zeta \in H^1(\Lambda).$$

Finally, H^n is defined as the restriction to Γ^n of $G^n/|\nabla\phi^n|$. Notice that this quantity is well defined since $|\nabla\phi^n|$ is not vanishing at the vicinity of Γ^n.

Let us consider the following Green formula on the closed surface Γ^n:

$$\int_{\Gamma^n} \Delta_s^n \xi\, \zeta \, \mathrm{d}s + \int_{\Gamma^n} \nabla_s^n \xi . \nabla_s^n \zeta \, \mathrm{d}s = 0, \ \forall \xi, \zeta \in H^1(\Gamma^n).$$

Then $Y^n = -\Delta H^n$ can be computed in a weak sense:

$$Y^n \in H^1(\Gamma^n) \ \text{ and } \ \int_{\Gamma^n} Y^n \, \zeta \, \mathrm{d}s = \int_{\Gamma^n} \nabla_s^n H^n . \nabla_s^n \zeta \, \mathrm{d}s, \ \forall \zeta \in H^1(\Gamma^n)$$

Let us summarize the procedure. The following additional bilinear forms are introduced:

$$\begin{aligned}
m_w^n(\phi,\psi) &= \int_\Lambda \varphi\, \psi \, |\nabla\phi^n| \, \mathrm{d}x, \ \forall \varphi, \psi \in L^2(\Lambda), \\
a_w^n(\phi,\psi) &= \int_\Lambda \nabla\varphi \, \nabla\psi \, |\nabla\phi^n| \, \mathrm{d}x, \ \forall \varphi, \psi \in H^1(\Lambda), \\
m_s^n(\xi,\zeta) &= \int_{\Gamma^n} \xi \ \zeta \, \mathrm{d}s, \ \forall \xi, \zeta \in L^2(\Gamma^n), \\
c^n(\xi,\zeta) &= \int_{\Gamma^n} \nabla_s^n \xi . \nabla_s^n \zeta \, \mathrm{d}s, \ \forall \xi, \zeta \in H^1(\Gamma^n).
\end{aligned}$$

Then, compute successively as:

$$\begin{aligned}
\mathbf{r}^n \in H_0(\mathrm{div},\Lambda) \text{ and } m(\mathbf{r}^n, \mathrm{s}) &= -b_1(|\nabla\phi^n|, \mathbf{s}^n), \ \forall \mathbf{s} \in H_0(\mathrm{div},\Lambda), \\
G^n \in H^1(\Lambda) \text{ and } m_w^n(G^n,\psi) &= a_w^n(\phi^n,\psi) + m(\mathbf{r}^n . \nabla\phi^n, \psi), \ \forall \psi \in H^1(\Lambda), \\
H^n &= \frac{G^n}{|\nabla\phi^n|} \ \text{ on } \ \Gamma^n, \\
Y^n \in H^1(\Gamma^n) \text{ and } m_s^n(Y^n,\zeta) &= c^n(H^n,\zeta), \ \forall \zeta \in H^1(\Gamma^n), \\
\mathbf{n}^n &= \frac{\nabla\phi^n}{|\nabla\phi^n|} \ \text{ on } \ \Gamma^n, \\
\mathbf{f}^n &= \frac{1}{Ca}\left(-Y^n + \frac{(H^n)^3}{2}\right)\mathbf{n}^n \ \text{ on } \ \Gamma^n.
\end{aligned}$$

3.2.3 Extension and regularization

The previous variational formulation involves integrals over the moving surface Γ^n: in order to avoid the explicit re-triangulation of the surface Γ^n at each time step, integrals over Γ^n are transformed into integrals over Λ. First, remarks that an integral over Γ^n can be written as an integral over Λ with the help of the level set function ϕ^n and the Dirac measure δ:

$$\int_{\Gamma^n} \varphi \, \mathrm{d}s = \int_\Lambda \tilde{\varphi} \ |\nabla\phi^n| \ \delta(\phi^n) \, \mathrm{d}x$$

where $\tilde{\varphi}$ is an extension to Λ of any function φ defined in Γ^n. Also, the normal vector $\mathbf{n}^n$, defined over Γ^n, extends as $\nabla\phi^n/|\nabla\phi^n|$ to Λ. Since there is no ambiguity, this extension of the normal is still denoted by $\mathbf{n}^n$. Also, the notations for the extension to Λ of the surface operators defined in (12) are still conserved. By this way, the Canham-Helfrich force, as expressed by (14), can be extended to Λ.

Nevertheless, the explicit management of Dirac measures is not an easy task in finite element methods. Thus, the previous extension is combined together with a

regularization procedure. Three sharp functions are here considered: the Heaviside function $\mathscr{H}(\phi^n)$, that acts as the indicator of $\Lambda\backslash\Omega^n$, the Dirac measure $\delta(\phi^n)$ that localizes the surface Γ^n, and the sign function $\mathrm{sgn}(\phi^n)$, that will be used in a forthcoming paragraph, for the redistancing of the level set function.

In order to avoid the triangulation of Γ^n, a banded region of width 2ε is introduced, for some $\varepsilon > 0$. The Heaviside $\mathscr{H}$, the Dirac δ and the sign functions are replaced respectively by $\mathscr{H}_\varepsilon$, δ_ε and sgn_ε, defined for all $\phi \in \mathbb{R}$ by:

$$\begin{aligned}
\mathscr{H}_\varepsilon(\phi) &= \begin{cases} 0, & \text{when } \phi < -\varepsilon, \\ \dfrac{1}{2}\left(1 + \dfrac{\phi}{\varepsilon} + \dfrac{\sin\left(\dfrac{\pi\phi}{\varepsilon}\right)}{\pi}\right), & \text{when } |\phi| \le \varepsilon, \\ 1, & \text{otherwise,} \end{cases} \\
\delta_\varepsilon(\phi) &= \frac{\mathrm{d}\mathscr{H}_\varepsilon}{\mathrm{d}\phi}(\phi) = \begin{cases} \dfrac{1}{2\varepsilon}\left(1 + \cos\left(\dfrac{\pi\phi}{\varepsilon}\right)\right), & \text{if } |\phi| \le \varepsilon \\ 0, & \text{otherwise} \end{cases} \\
\mathrm{sgn}_\varepsilon(\phi) &= 2\mathscr{H}_\varepsilon(\phi) - 1
\end{aligned}$$

The sharp viscosity is also replaced by a smooth one:

$$\eta^n_{*,\varepsilon} = \beta + (1-\beta)\mathscr{H}_\varepsilon\left(\phi^n\right)$$

The previous bilinear forms admits a regularized counterpart:

$$\begin{aligned}
a^n_\varepsilon(\mathbf{u},\mathbf{v}) &= \int_\Lambda 2\,\eta^n_{*,\varepsilon}\, D(\mathbf{u}) : D(\mathbf{v})\,\mathrm{d}x,\ \forall \mathbf{u},\mathbf{v} \in \left(H^1(\Lambda)\right)^2, \\
m^n_{s,\varepsilon}(\mathbf{u},\mathbf{v}) &= \int_\Lambda \mathbf{u}.\mathbf{v}\,|\nabla\phi^n|\,\delta_\varepsilon\left(\phi^n\right)\,\mathrm{d}x,\ \forall \mathbf{u},\mathbf{v} \in \left(L^2(\Lambda)\right)^2, \\
b^n_{2,\varepsilon}(\mathbf{v},\mu) &= -\int_\Lambda \mu\,\mathrm{div}^n_s\,\mathbf{v}\,|\nabla\phi^n|\,\delta_\varepsilon\left(\phi^n\right)\,\mathrm{d}x,\ \forall \mu \in L^2(\Lambda),\ \forall \mathbf{v} \in \left(H^1(\Lambda)\right)^2, \\
c^n_\varepsilon(\xi,\zeta) &= \int_\Lambda \nabla^n_s\xi.\nabla^n_s\zeta\,|\nabla\phi^n|\,\delta_\varepsilon\left(\phi^n\right)\,\mathrm{d}x,\ \forall \xi,\zeta \in H^1(\Lambda)
\end{aligned}$$

The computation of the curvature H^n is unchanged while the Canham-Helfrich force becomes: find $Y^n_\varepsilon \in H^1(\Lambda)$ such that

$$m_{s,\varepsilon}(Y^n_\varepsilon,\zeta) = c_\varepsilon(H^n,\zeta),\ \forall \zeta \in H^1(\Lambda).$$

Then, compute the extension to Λ of the force:

$$\mathbf{f}^n_\varepsilon = \frac{1}{Ca}\left(-Y^n_\varepsilon + \frac{(H^n)^3}{2}\right)\mathbf{n}^n \ \text{ in } \Lambda.$$

Problem (15) admits a regularized variant:

$(S)_\varepsilon$: *find* $\mathbf{u}^n_\varepsilon \in \mathbb{V}(\mathbf{u}_b)$, $p^n_\varepsilon \in L^2(\Lambda)$ *and* $\lambda^n_\varepsilon \in L^2(\Lambda)$ *such that*

$$\begin{aligned}
&\frac{3Re}{2\Delta t} m\left(\mathbf{u}^n_\varepsilon,\mathbf{v}\right) + a^n_\varepsilon\left(\mathbf{u}^n_\varepsilon,\mathbf{v}\right) + b_1\left(\mathbf{v},p^n_\varepsilon\right) + b^n_{2,\varepsilon}\left(\mathbf{v},\lambda^n_\varepsilon\right) \\
&= m^n_{s,\varepsilon}\left(\mathbf{f}^n_\varepsilon,\mathbf{v}\right) + \frac{Re}{2\,\Delta t} m\left(4\mathbf{u}^n_\varepsilon oX^n_2 - \mathbf{u}^{n-1}_\varepsilon oX^{n-1}_2,\mathbf{v}\right), \qquad (16a) \\
&b_1\left(\mathbf{u}^n_\varepsilon,q\right) = 0, \qquad (16b) \\
&b^n_{2,\varepsilon}\left(\mathbf{u}^n_\varepsilon,\mu\right) = 0, \qquad (16c)
\end{aligned}$$

for all $\mathbf{v} \in \mathbb{V}(0)$, $q \in L^2(\Lambda)$ and $\mu \in L^2(\Lambda)$. Notice that the surface tension λ^n_ε is now extended to Λ. The regularization parameter ε will be chosen as proportional to the the mesh size h, as presented in the next paragraph.

3.2.4 Finite element discretization

The Taylor-Hood finite element approximation (see e.g. [7]) for the Stokes problem is considered here for the velocity-pressure approximation of the generalized Stokes problem. Let $\mathscr{T}_h$ a finite element triangulation of Λ, where $h > 0$ stands for the largest element diameter [6]. The following finite dimensional spaces are introduced:

$$\begin{aligned} X_h &= \left\{ q \in C^0\left(\overline{\Lambda}\right),\ q_{|K} \in \mathbb{P}_1,\ \forall K \in \mathscr{T}_h \right\}, \\ \mathbf{S}_h &= \left\{ \mathbf{s} \in X_h^2,\ \mathbf{s}.\boldsymbol{\nu} = 0 \text{ on } \partial\Lambda \right\}, \\ \mathbb{X}_h &= \left\{ \mathbf{u} \in \left(C^0\left(\overline{\Lambda}\right)\right)^2,\ \mathbf{u}_{|K} \in (\mathbb{P}_2)^d,\ \forall K \in \mathscr{T}_h \right\}, \\ \mathbb{V}_h(\mathbf{u}_b) &= \mathbb{X}_h \cap \mathbb{V}(\mathbf{u}_b). \end{aligned}$$

Let us assume that $\phi_h^n \in X_h$ is an approximation of ϕ^n at the n-th time step. The computation of the discrete Canham-Helfrich force write:

$$\begin{aligned} \mathbf{r}_h^n \in S_h \text{ and } m(\mathbf{r}_h^n, \mathrm{s}) &= -b_1(|\nabla\phi_h^n|,\ \mathbf{s}^n),\ \forall \mathbf{s} \in S_h, \\ G_h^n \in X_h \text{ and } m_w^n(G_h^n, \psi) &= a_w^n(\phi_h^n, \psi) + m(\mathbf{r}_h^n.\nabla\phi_h^n, \psi),\ \forall \psi \in X_h, \\ H_h^n &= \frac{G_h^n}{|\nabla\phi_h^n|} \ \text{ in } \ \Lambda, \\ Y_h^n \in X_h \text{ and } m_{s,\varepsilon}(Y_h^n, \zeta) &= c_\varepsilon(H_h^n, \zeta),\ \forall \zeta \in X_h, \\ \mathbf{n}_h^n &= \frac{\nabla\phi_h^n}{|\nabla\phi_h^n|} \ \text{ in } \ \Lambda, \\ \mathbf{f}_h^n &= \frac{1}{Ca}\left(-Y_h^n + \frac{(H_h^n)^3}{2}\right)\mathbf{n}_h^n \ \text{ in } \ \Lambda. \end{aligned}$$

The discrete generalized Stokes problem writes:

$(S)_h$: *find* $\mathbf{u}_h^n \in \mathbb{V}_h(\mathbf{u}_b)$, $p_h^n \in X_h$ *and* $\lambda_h^n \in X_h$ *such that*

$$\begin{aligned} &\frac{3Re}{2\Delta t} m\left(\mathbf{u}_h^n, \mathbf{v}\right) + a_\varepsilon^n\left(\mathbf{u}_h^n, \mathbf{v}\right) + b_1\left(\mathbf{v}, p_h^n\right) + b_{2,\varepsilon}^n\left(\mathbf{v}, \lambda_h^n\right) \\ &= m_{s,\varepsilon}^n\left(\mathbf{f}_h^n, \mathbf{v}\right) + \frac{Re}{2\,\Delta t} m\left(4\mathbf{u}_h^{n-1} o X_2^{n-1} - \mathbf{u}_h^{n-2} o X_2^{n-2}, \mathbf{v}\right), \qquad (17a) \\ &b_1\left(\mathbf{u}_h^n, q\right) = 0, \qquad (17b) \\ &b_{2,\varepsilon}^n\left(\mathbf{u}_h^n, \mu\right) = 0. \qquad (17c) \end{aligned}$$

for all $\mathbf{v} \in \mathbb{V}_h(0)$, $q \in X_h$ and $\mu \in L_h$. The previous finite-dimensional linear system involves the following matrix structure:

$$\begin{pmatrix} A & B_1^T & B_2^T \\ B_1 & 0 & 0 \\ B_2 & 0 & 0 \end{pmatrix}$$

Such systems has been extensively studied and various efficient strategies are known (see e.g. [14]). In the present paper, this system is solved efficiently by the preconditioned conjugate gradient algorithm, as implemented in the Rheolef C++ library [32].

3.3 The transport subproblem

3.3.1 Redistanciation

The transport, as defined in (4) deforms the initial level function ϕ, which is not any more a signed distance for $t > 0$. As a consequence, an auxiliary problem called

the *redistancing problem* has to be solved in order to keep the function ϕ near a signed distance. The redistancing step can be expressed, for all $t \in]0,T[$, as an advection problem depending on a pseudo-time τ and we shall find the stationary solution (see [25] for more details). Let $\tilde{\phi}(t,.)$ be the level set function at time t that is no more a distance function. Let us introduce the vector field $\mathbf{v} = \operatorname{sgn}\left(\tilde{\phi}\right)\dfrac{\nabla\psi}{|\nabla\psi|}$. Then, the redistancing problem expresses as:

$$\left\{\begin{array}{rll} \dfrac{\partial\psi}{\partial\tau}(\tau,x;t) + \mathbf{v}.\nabla\psi & = \operatorname{sgn}\left(\tilde{\phi}\,(t,x)\right) + \lambda(\tau,x:t)\,g(\psi) & \text{a.e. } (\tau,x) \in]0,+\infty[\times\Lambda, \\ \psi(0,x;t) & = \tilde{\phi}(x,t) & \text{a.e. } x \in \Lambda. \end{array}\right. \tag{18}$$

where $\operatorname{sgn}\left(\tilde{\phi}\right)$ denotes the sign function and is equal to $0,-1,+1$ respectively on $\Gamma(t)$, in $\Gamma(t)$ and outside $\Gamma(t)$. We note also that $\lambda(\tau,x;t)$ is a Lagrange multiplier that enforces the constraint of constant volume locally at $x \in \Lambda$. We chose $g(\psi) = \delta(\psi)|\nabla\psi|$, the Lagrange multiplier has an explicit average value $\lambda_{\mathcal{V}}$ over an arbitrary *finite volume* $\mathcal{V} \subset \Lambda$:

$$\lambda_{\mathcal{V}}(\tau;t) \quad = \quad \left\{\begin{array}{ll} \dfrac{\int_{\mathcal{V}} \delta(\psi)\,\left(\mathbf{v}.\nabla\psi - \operatorname{sgn}\left(\tilde{\phi}\right)\right)\,\psi x}{\int_{\mathcal{V}} \delta(\psi)\,g(\psi)\,\mathrm{d}x} & \text{when } \mathcal{V}\cap\Gamma(t) \neq \emptyset \\ 0 & \text{otherwise} \end{array}\right. \tag{19}$$

The stationary solution satisfies $|\nabla\psi| = 1$ almost everywhere in Λ, consequently $\psi(\infty,.;t)$ is a signed distance and is taken as the new level set function $\phi(t,.)$ at time t. Let us notice that the solution ψ of the redistancing problem (18) preserve the position of $\Gamma(t)$: for any $\tau > 0$, the zero level set of $\psi(\tau,.;t)$ is the same zero level set of $\phi(t,.)$. As a result the volume $\operatorname{meas}(\Omega(t))$ is also preserved, this point has great importance for numerous applications. However, after discretization by finite difference or finite element methods, this property is satisfied only approximately. Let us introduce the `redistance` operator defined by $\phi(t,.) = \texttt{redistancing}(\tilde{\phi}(t,.))$.

Let $\tilde{\phi}^n$ be the approximation of $\tilde{\phi}(t)$, at time t^n and $\psi^m, \mathbf{v}^m$ be approximations of $\psi(\tau), \mathbf{v}(\tau)$ respectively at τ^m. The time discretization is performed by using the method of characteristics and the total derivative $D\psi/Dt$ is approximated by a first-order backward Euler scheme as previously. The redistancing problem (18) is solved explicitly:

$$\psi^{m+1} = \left\{\begin{array}{ll} \psi^m & \text{when } |\tilde{\phi}^n| < \varepsilon \\ \psi^m \circ X^m_{\mathbf{v}_\varepsilon} + \Delta\tau\ \operatorname{sgn}_\varepsilon(\tilde{\phi}^n) & \text{otherwise} \end{array}\right. \tag{20}$$

Here, the characteristic have subscripts $\mathbf{v}_\varepsilon$ in order to avoid confusion. Let W_h be the space of piecewise constant functions on $\mathcal{T}_h$ and π_h denotes the Lagrange interpolation in Q_h. Let $\psi^0_h = \tilde{\phi}^{n+1}_h$. At any step $m \geq 0$ of the redistancing algorithm, suppose $\psi^m_h \in Q_h$ being known, and let $\mathbf{g}^m_h \in Q^N_h$ be the approximation of $\nabla\psi^m_h \in W^N_h$ defined by the following linear system:

$$\int_\Lambda \mathbf{g}^m_h.\boldsymbol{w}_h\,\mathrm{d}x = \int_\Lambda \nabla\psi^m_h.\boldsymbol{w}_h\,\mathrm{d}x, \quad \forall \boldsymbol{w}_h \in Q^N_h$$

A mass lumping procedure is used for this linear system: the integrals involved in the computation of the coefficients of the matrix associated to the L^2 scalar product are evaluated by using the trapeze quadrature formulae. By this way, the matrix of the linear system is replaced by a diagonal one, and the computation of $\mathbf{g}^m_h$ becomes explicit. Then, let

$$\mathbf{v}^m_{\varepsilon,h} = \pi_h\left(\operatorname{sgn}_\varepsilon\left(\tilde{\phi}^{n+1}_h\right)\frac{\mathbf{g}^m_h}{|\mathbf{g}^m_h|}\right)$$

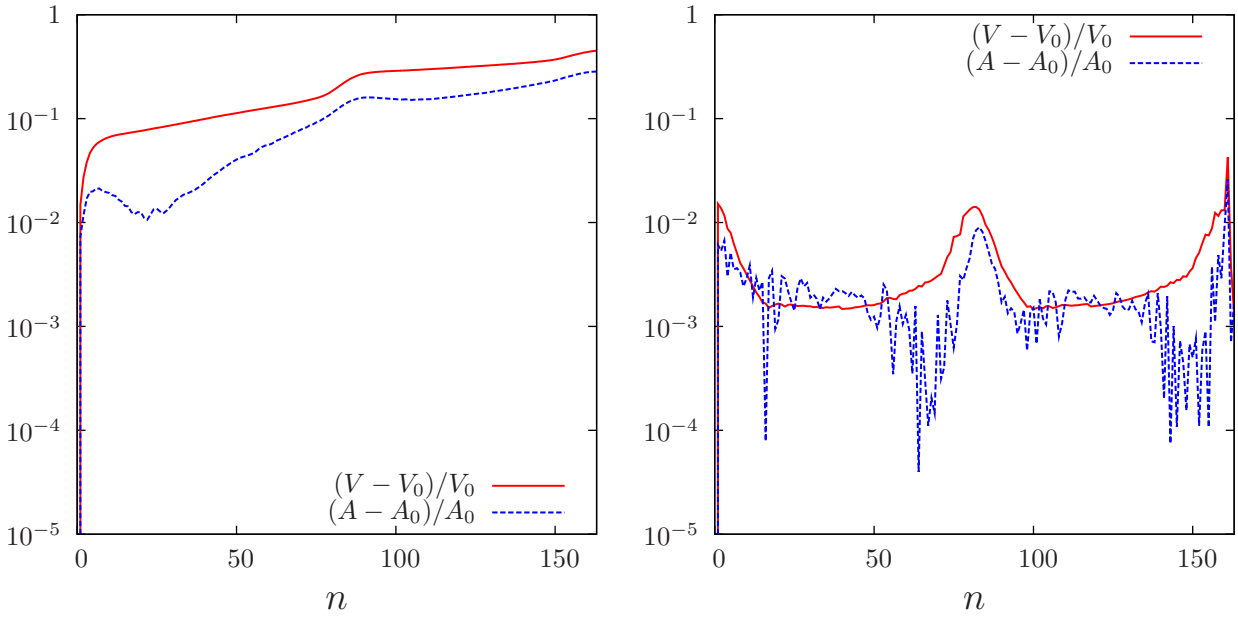

Figure 2: The vesicle area and perimeter errors, for $h = 5.3 \times 10^{-2}$, $\Delta t = 3 \times 10^{-2}$, $\tau = 0.81$ and $\varepsilon = 2.5\, h$: (a) without and (b) with Lagrange multipliers.

The discrete version of the redistancing algorithm writes also explicitly:

$$\psi_h^{m+1} = \begin{cases} \psi_h^m & \text{when } |\tilde{\phi}_h^n| < \varepsilon \\ \pi_h \left\{ \psi_h^m \circ X_{\mathbf{v}_\varepsilon}^m + \Delta\tau \ \mathrm{sgn}_\varepsilon(\tilde{\phi}_h^n)(1 - |\nabla \psi_h^m|) \right\} & \text{otherwise} \end{cases} \tag{21}$$

3.3.2 Improvement of the area and perimeter conservations

Let us summarize here the resolution of the problem:

Algorithm 1

- $n = 0$: Let $\Gamma(0)$ be the initial shape and ϕ_h^0 be its associated signed distance function. Let $\mathbf{u}_h^0 = \mathbf{u}_h^{-1} \in \mathbb{V}(\mathbf{u}_b)$ be the initial velocity field.
- $n \geq 1$: Let $\phi_h^{n-1} \in Q_h$ and $\mathbf{u}_h^{n-1}$, $\mathbf{u}_h^{n-2} \in \mathbb{V}_h(\mathbf{u}_b)$ being known. Then

  step 1 : compute $\tilde{\phi}_h^n = \pi_h \left(\phi_h^{n-1} \circ X_1^{n-1} \right) \in Q_h$;

  step 2 : compute $\phi_h^n = \texttt{redistancing}(\tilde{\phi}_h^n)$;

  step 3 : compute $\mathbf{u}_h^n$, p_h^n and λ_h^n from (17).

In this section we present a numerical simulation to illustrate the features of the numerical method. We choose $Re = 10^{-3}$, $Ca = 10^3$, $\alpha = 1/10$, $\tau = 0.81$ and a viscosity rate $\beta = 50$. Fig. 2.a plots the evolution of the relative error in vesicle area and perimeter. Observe that, after few iterations, the error becomes higher than 10% of the reference vesicle area and perimeter: this error completely changes the vesicle, that evolves to a circular shape. The algorithm must be modified in order to improve the area and perimeter conservation. The problem of advection (4a) is

substituted by the equivalent system:

$$\frac{\partial \phi}{\partial t} + \left[\mathbf{u} + (p_* + \lambda_* f)\,\mathbf{n}\right].\nabla\phi = 0 \quad \text{a.e } (t,x) \in]0,+\infty[\times\Lambda\,, \tag{22}$$

$$\frac{\mathrm{d}}{\mathrm{d}t}\int_\Lambda (1-\mathscr{H}(\phi))\,\mathrm{d}x = 0 \quad \forall t \in]0,+\infty[\,, \tag{23}$$

$$\frac{\mathrm{d}}{\mathrm{d}t}\int_{\partial\Omega} \mathrm{d}s = 0 \quad \forall t \in]0,+\infty[\,, \tag{24}$$

where p_* and λ_* are two global Lagrange multipliers associated to two additional constraints for area and perimeter preservation. This system leads, after time discretization, to a modified and more robust scheme, with a modified advection field $\mathbf{u}_* = \mathbf{u} + (p_* + \lambda_* f)\,\mathbf{n}$. The variation of area $V(t)$ at time t^n writes:

$$\frac{\mathrm{d}V}{\mathrm{d}t}(t^n) = \left[\frac{\mathrm{d}}{\mathrm{d}t}\int_\Lambda (1-\mathscr{H}(\phi))\,\mathrm{d}x\right]_{t=t^n} = \frac{V^n - V^{n-1}}{\Delta t} + \mathcal{O}(\Delta t)\,, \tag{25}$$

where $V^{n-1} = \int_{\Omega^{n-1}} \mathrm{d}x$ is known and we want to impose that $V^n = V_0$ the initial area, in order to avoid the previous area error accumulation. Conversely, the variation of the perimeter $A(t)$ at time t^n expresses:

$$\frac{\mathrm{d}A}{\mathrm{d}t}(t^n) = \left[\frac{\mathrm{d}}{\mathrm{d}t}\int_{\partial\Omega} \mathrm{d}s\right]_{t=t^n} = \frac{A^n - A^{n-1}}{\Delta t} + \mathcal{O}(\Delta t)\,, \tag{26}$$

where $A^{n-1} = \int_{\partial\Omega^{n-1}} \mathrm{d}s$ is known and we want to impose that $A^n = A_0$ the initial perimeter. Combining (22) and (23), we obtain:

$$\frac{\mathrm{d}}{\mathrm{d}t}\int_\Lambda (1-\mathscr{H}(\phi))\,\mathrm{d}x = -\int_\Lambda \frac{\partial\phi}{\partial t}\delta(\phi)\,\mathrm{d}x = -\int_{\partial\Omega}\frac{1}{|\nabla\phi|}\frac{\partial\phi}{\partial t}\,\mathrm{d}s = \int_{\partial\Omega}\frac{1}{|\nabla\phi|}\mathbf{u}_*.\nabla\phi\,\mathrm{d}s\,. \tag{27}$$

Recall that, for any function φ and vector field $\mathbf{v}$, the Reynolds formulæ on a surface Γ writes:

$$\frac{\mathrm{d}}{\mathrm{d}t}\int_\Gamma f\,\mathrm{d}s = \int_\Gamma \frac{\mathrm{d}f}{\mathrm{d}t} + \nabla.(f\,\mathbf{u}) - f(\nabla\mathbf{u}.\mathbf{n}).\mathbf{n}\,\mathrm{d}s\,. \tag{28}$$

With $\varphi = 1$ and $\mathbf{v} = \mathbf{u}_*$, and using the Green formulæ (8), we get successively:

$$\frac{\mathrm{d}}{\mathrm{d}t}\int_{\partial\Omega}\mathrm{d}s = \int_{\partial\Omega}\mathrm{div}_s\,\mathbf{u}_*\,\mathrm{d}s = \int_{\partial\Omega} H\,\mathbf{u}_*.\mathbf{n}\,\mathrm{d}s. \tag{29}$$

At time t^n, replacing $\mathbf{u}_*^n$ by $\mathbf{u}^n + (p_*^n + \lambda_*^n f)\,\mathbf{n}^n$ in (25)-(26) and using (27)-(29), we obtain the following linear system with two unknowns $(p_*^n, \lambda_*^n) \in \mathbb{R}^2$:

$$\begin{aligned} p^*\int_{\partial\Omega}\mathrm{d}s + \lambda^*\int_{\partial\Omega} f\,\mathrm{d}s &= \frac{V_0 - \int_{\Omega^n}\mathrm{d}x}{\Delta t} - \int_{\partial\Omega}\mathbf{u}.\mathbf{n}\,\mathrm{d}s\,, \\ p^*\int_{\partial\Omega} H\,ds + \lambda^*\int_{\partial\Omega} H\,f\,\mathrm{d}s &= \frac{A_0 - \int_{\partial\Omega^n}\mathrm{d}s}{\Delta t} - \int_{\partial\Omega} H\,\mathbf{u}.\mathbf{n}\,\mathrm{d}s\,. \end{aligned}$$

Choosing f a non-constant function ensure that this system is well-posed. In our simulations, we use $f(x_1,x_2) = 2x_1^2 + x_2^2$.

The numerical parameter for the simulation of the vesicle in the linear shear flow are the same as those of Fig. 2.a, and now the area and perimeter corrections for the advection step are used. Results are shown on Fig. 2.b: observe that the area and perimeter are well conserved. The relative error is of about 0.1% and remains bounded along iterations.

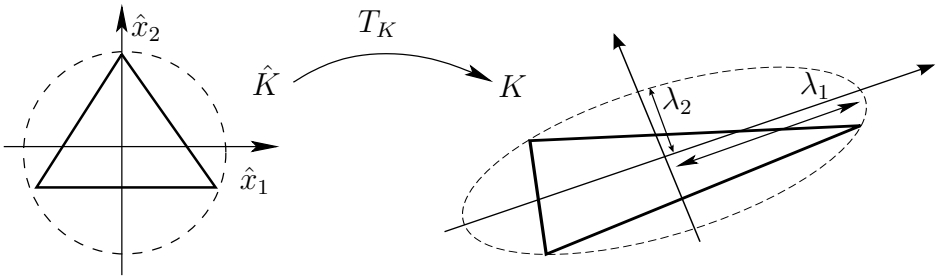

Figure 3: Transformation from the reference element $\hat{K}$ to any triangle K.

3.3.3 Improvement by mesh adaptation

A way to adapt the mesh to the computation of a governing field is to equi-distribute its interpolation error, i.e. to make it constant over all triangles and in the directions of maximal and minimal stretching and to adjust the maximal and minimal directions of stretching to others of maximal and minimal error. Our approach bases on the bidirectional anisotropic mesh generator `bamg` developed by F. Hecht [17] (see also [32, 18, 19]), together with the choice of a particular metric, specific to our time-dependent level set problem.

For any triangle K of the mesh $\mathcal{T}_h$ at time t, let T_K be the affine transformation which maps the reference triangle $\hat{K}$ into K (see Fig. 3):

$$\begin{array}{rccl} T_K: & \hat{K} & \longrightarrow & K \\ & \hat{x} & \longmapsto & \mathbf{x} = T_K(\hat{\mathbf{x}}) = M_K \hat{\mathbf{x}} + \mathbf{t}_K\,. \end{array}$$

where M_K is the Jacobian of T_K. Notice that M_K is unsymmetric and invertible, otherwise K would be flat. Thus, M_K admits a singular value decomposition (for SVD, see [16, p. 69]): $M_K = R_K^T \Lambda_K P_K$, where R_K and P_K are orthogonal and where Λ_K is diagonal with positive entries. The choice of the reference triangle $\hat{K}$ is not unique. It is common practice to choose as $\hat{K}$ the right triangle $\{(x_1, x_2), x_1 > 0, x_2 > O, x_1 + x_2 < 1\}$. For mesh generation and adaption purposes, an equilateral triangle, inscribed in the unit circle, is often preferred [13]. Since $\hat{x} = M_K^{-1}(x - t_K)$, the unit circle equation $\hat{x}^T \hat{x} = 1$ becomes:

$$1 = (x - t_K)^T M_K^{-T} M_K^{-1} (x - t_K) = (x - t_K)^T R_K^T \Lambda_K^{-2} R_K (x - t_K)$$

This is the equation of an ellipse containing K (see Fig. 3).

Following [17], our choice of the metric is based on the hessian tensor of a specific governing field χ, for which we aim at decreasing the interpolation error. The interpolation error in the direction $\mathbf{v} \in \mathbb{R}^2$ is given by:

$$e_{K,\mathbf{v}} = h_{K,\mathbf{v}}^2 \left\| \frac{\partial^2 \chi}{\partial \mathbf{v}^2} \right\| \quad \text{on } K,$$

where $h_{K,\mathbf{v}}$ denotes the length of K in the direction $\mathbf{v}$ and $\dfrac{\partial^2 \chi}{\partial \mathbf{v}^2} = \mathbf{v}^T \nabla\nabla\chi\, \mathbf{v}$, and $\nabla\nabla\chi$ is the hessian matrix of χ.

By adjusting the directional sizes $h_{K,\mathbf{v}}$ of K for each eigenvector of the hessian matrix and each element K, the local directional interpolation errors can be equidistributed on the whole domain. An adaptation loop is required in order to assure the convergence of both the approximation of χ and its corresponding mesh. In order

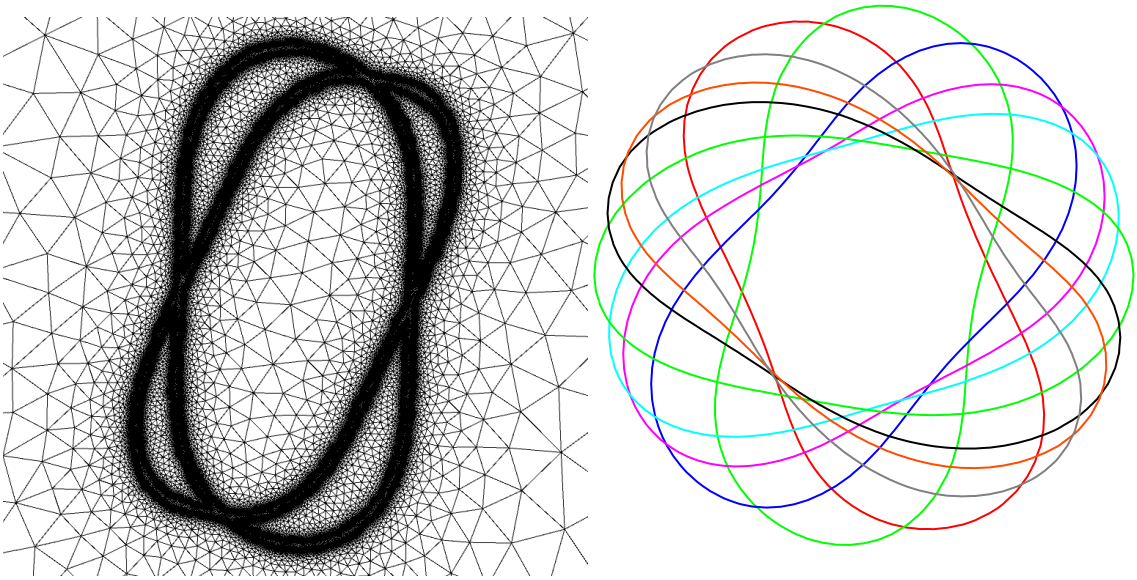

Figure 4: (a) Zoom on the adapted mesh ; (b) Vesicle tumbling under a linear shear flow for $\alpha = 1/4$, $\beta = 20$, $Ca = 10^4$ and $Re = 10^{-3}$. The shapes are shown for $t = kT_p/14$, $k \in \{1, 2, 3, 4, 5, 8, 11, 12, 13\}$, where $T_p = 10.3$ is the tumbling period.

to adapt the mesh to the vesicle boundary $\partial\Omega^n$ at each time step t_n, the governing field $\chi = \delta_\varepsilon(\phi^n) + \delta_\varepsilon(\phi^{n-1})$ has been chosen for the adaptation loop. For an uniform mesh, the regularization parameter used for the computation of integrals over $\partial\Omega$ is chosen as proportional to the element size: $\varepsilon = 2h$. This choice is extended to a non-uniform mesh with a non-constant $\varepsilon(x)$, $x \in \Lambda$, that is proportional to an average value of the local mesh size: $\varepsilon(x) = 2\sqrt{2}\,\mathrm{meas(K)}^{\frac{1}{2}}$, for all $x \in K$. Fig. 4.a shows a zoom on the adapted mesh at the end of the adaptation loop, where both the contours of $\partial\Omega^{n-1}$ and $\partial\Omega^n$ are captured. Fig. 4.b represents the vesicle boundary evolution, as computed by the present auto-adaptive procedure.

4 Numerical results

4.1 Vesicles in the tumbling mode

Simulations show, in accord with literature, that two flow regimes exist: a steady-state tank-treading regime where the vesicle assumes a steady-state shape and its inclination angle remains constant with time, while the fluid membrane undergoes a tank-tread-like regime; the other is a tumbling regime where the vesicle rotates along the flow vorticity direction axis, and the regime is periodic in time. The transition between the two regimes for a vesicle of fixed reduced area γ happens at a critical viscosity ratio between the inside and outside fluid, beyond which the vesicle tumbles.

Along this part, we are interested on small Reynolds number. It is the typical situation in microfluidic devices and the viscous forces are dominant over the inertial ones, the flow is almost laminar, and no turbulence can be observed, at least in the absence of vesicle. We choose the following parameters: $Re = 10^{-4}$, $Ca = 10^3$, $\Upsilon = 20$ and a vesicle with a reduced area $\gamma = 0.89$ and we choose a time step $\Delta t = 2.5 \times 10^{-3}$.

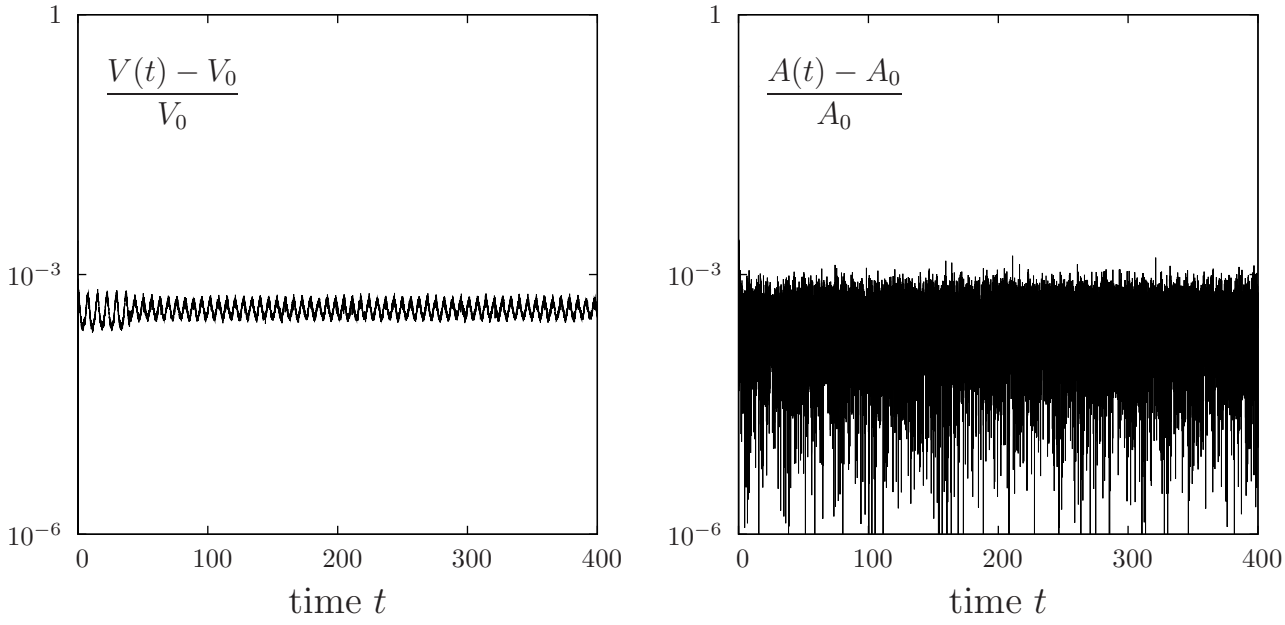

Figure 5: Area and perimeter preservation versus time t with $\Delta t = 2.5 \times 10^{-3}$: (a) the vesicle area; (b) the vesicle perimeter.

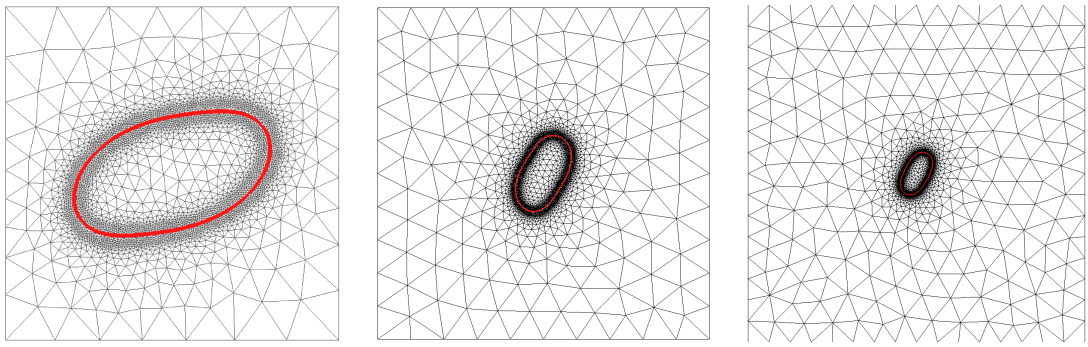

Figure 6: Mesh used for the study of the confinement α: left: $\alpha = 1/2$; middle: $\alpha = 1/5$; right: $\alpha = 1/9$.

In their experimental tests, Vitkova and al. [34] use vesicles with a diameter $50\eta m$ in a canal with a length $1mm$, this leads to a confinement $1/20$. In this section, the viscosity ratio α is chosen such that the vesicle is in a tumbling mode. We note that we use confinements between $1/2$ and $1/5$ in the case of a regular mesh. In the case of adapted mesh, the confinement can reach $1/12$. Based on the correction procedure introduced in the previous section, computations are performed with $\alpha = 1/9$ and Fig. 5 plots the evolution of relative mass errors $(V - V_0)/V_0$ and $(A - A_0)/A_0$. Observe that, over a duration equivalent to 80 periods of tumbling, both the area and perimeter relative errors remains bounded by 10^{-3}.

Let us now investigate the effect of the confinement α on the tumbling regime of the vesicle. Meshes used for different confinements are shown in Fig. 6 as well as the vesicle boundary $\partial\Omega$. Fig. 7 plots the evolution of the tumbling period, denoted as T_p, versus $1/\alpha$. As it could be expected, these results show that when the confinement α decreases, the tumbling period becomes independent of α. In the simulations presented in the rest of the paper, $\alpha = 1/4$ was chosen, since the

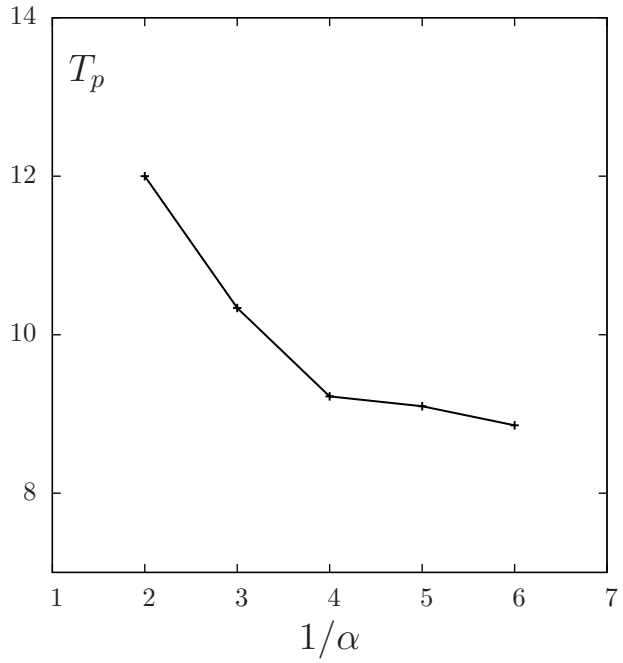

Figure 7: Tumbling period T_p versus $1/\alpha$ for $\gamma = 0.82$.

solution it sufficiently independent of the confinement. Let us denote by $\theta(t)$ the inclination angle measured counterclockwise from the positive x_1 semi-axis. The numerical computation of the inclination angle $\theta(t)$ for an arbitrary shape $\Omega(t)$ is reported in appendix C. The vesicle reaches a periodic regime after about 10 periods of tumbling: the inclination angle $\theta(t)$ becomes periodic. Let us observe on Fig. 8 some Lissajous representations, suitable for periodic phenomenas. The solution is represented, during the 10^{th} period, where the periodic regime is well established. Fig. 8.a the angular velocity $\frac{d\theta}{dt}$ versus θ: observe that the angular velocity is minimal when $\theta = 0$, i.e. when the vesicle is aligned with the horizontal axis, while its maximal when the vesicle is aligned vertically ($\theta = \pm\pi/2$). Fig. 8.b the evolution of the Canham-Helfrich energy versus θ: this energy reaches a global maximum when the vesicle is roughly aligned horizontally and, conversely, reaches a minimum when its roughly aligned vertically. Here, there is a small phase shift: the extrema of the energy are slightly in advance with the corresponding extrema of the angular velocity.

In order to study analytically the dynamics of vesicles, a rough analytical model was proposed in 1982 by Keller and Skalak [21]. This model incorporates a quasi-inextensible membrane, but vesicles were treated as undeformable liquid ellipsoids. Nevertheless, this model was able to reproduce tumbling regime notably for reduced area γ near 1 (i.e. quasi-spherical shapes), for which the distance to inextensibility is weak. Keller and Skalak [21] showed that the ellipsoid motion is described by:

$$\frac{\mathrm{d}\theta}{\mathrm{d}t} = -\frac{1}{2} + c(\gamma\,,\,\beta)cos(2\theta),$$

where $c(\gamma\,,\,\beta)$ is a coefficient depending on the aspect ratio γ and the viscosity ratio β. Fig. 9 plots $\frac{\mathrm{d}\theta}{\mathrm{d}t}$ versus $cos(2\theta)$. Observe the good correspondence with the affine behavior, as predicted by the Keller and Skalak theory. A linear regression on the numerical simulation data leads to the slope coefficient $c = 0.33$.

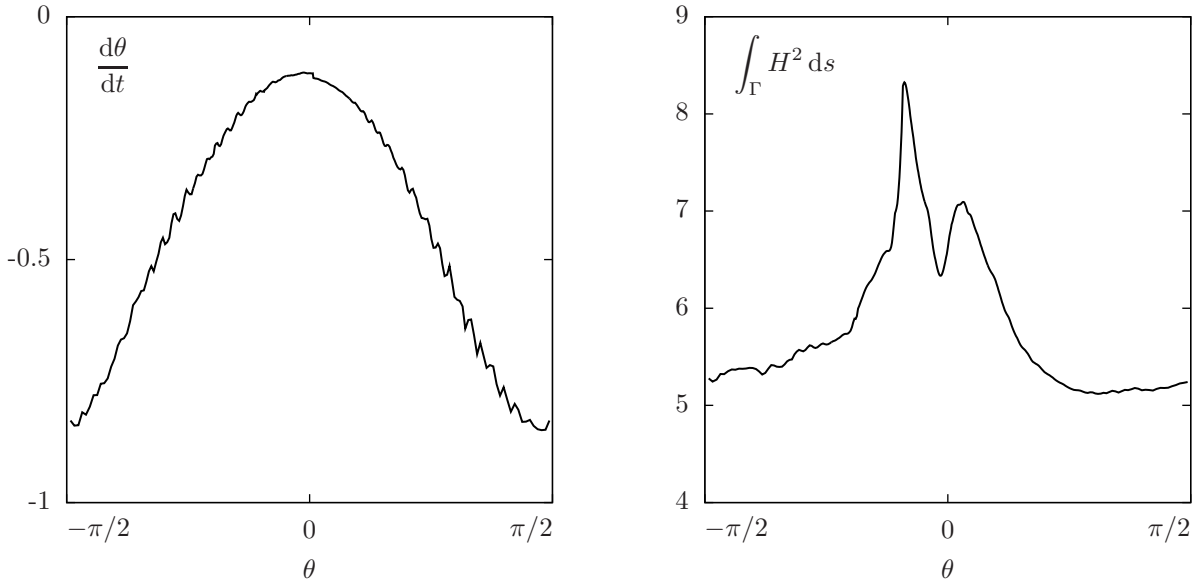

Figure 8: Lissajous curves: (a) the angular velocity $\frac{d\theta}{dt}$ versus θ et (b) the Canham-Helfrich energy versus θ.

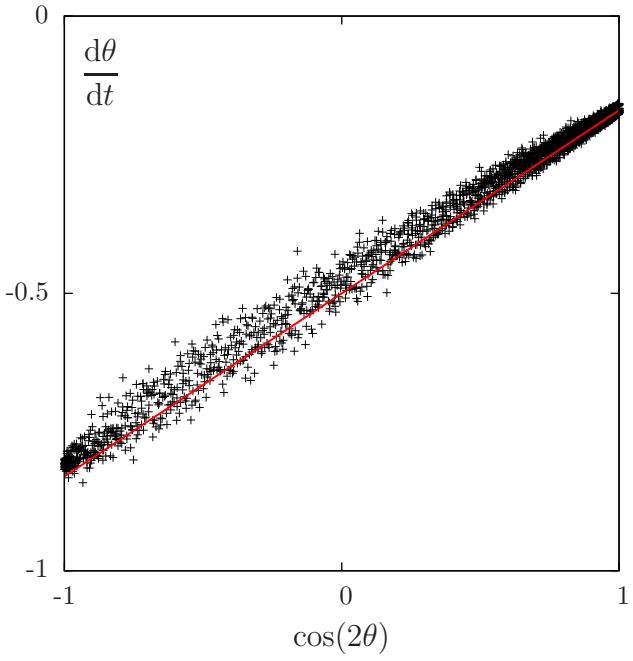

Figure 9: Plot of $\frac{d\theta}{dt}$ versus $cos(2\theta)$ for $\gamma = 0.84\,, \beta = 50\,, Re = 10^{-4}\,, Ca = 10^4$ and a confinement $\alpha = 1/9$. A linear regression leads to $\frac{d\theta}{dt} = 0.33\,cos(2\theta) - 0.5$, as indicated by the continuous line.

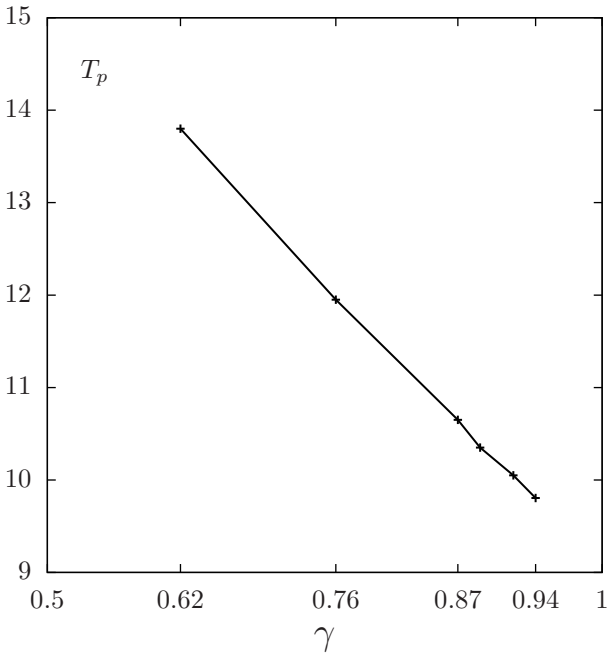

Figure 10: Tumbling period T_p function of the reduced area γ, with $\beta = 50$, $Re = 10^{-4}$ and $Ca = 10^3$.

Let us turn to the effect of the reduced area γ on the period of tumbling T_p. We consider a vesicle with a viscosity ratio $\beta = 50$ in a shear flow with a Reynolds number $Re = 10^{-4}$ and a Capillarity number $Ca = 10^3$. Observe on Fig. 10 a quasi-linear dependence of T_p upon γ.

4.2 The tank-treading regime

When the viscosity contrast tends to the critical value of viscosity, a transition to the tank-treading regime occurs. When the viscosity contrast β is small, the fluid inside the vesicle is highly deformed and rotated, and the vesicle adopts a stationary boundary $\partial\Omega$; its orientation $\theta(t)$ reaches rapidly a stationary value θ^* (see Fig. 11.a) Notice that the velocity is not vanishing along $\partial\Omega$: the membrane continue to tread like a tank and the internal fluid follow this rotation. Fig. 11.b plots the dependence of θ^* upon γ. Observe that θ^* increases versus γ.

Fig. 12 plots the streamlines and the velocity fields on the vesicle membrane. Remark that, when the stationary regime is reached, the velocity is tangential to the membrane.

4.3 Effect of inertia

An exhaustive study of the rheology of a vesicle in the presence of inertia has been carried out in this section. Although the basic behaviors had already been observed, the results shown in this part were nontrivial and not completely understood yet. For red blood cells in an blood vessel, the Reynolds number Re is not always very small so the Stokes limit is not always available: R_0 is about 3×10^{-6} m η_0 is

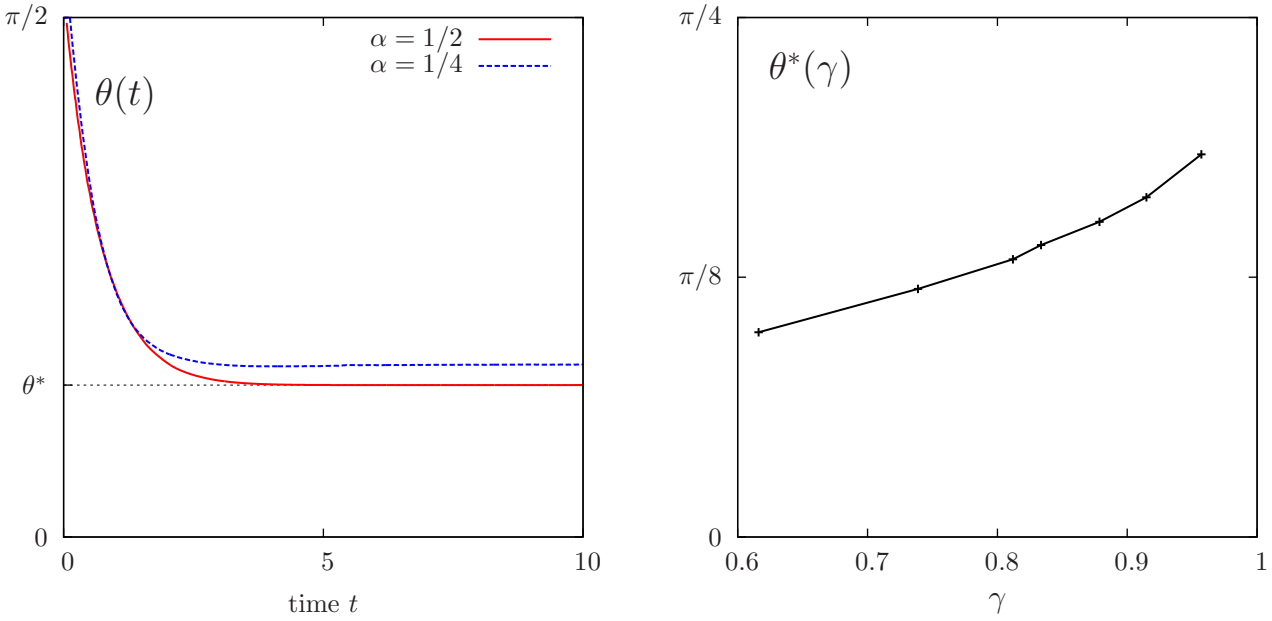

Figure 11: Tank-treading regime for $\gamma = 0.84$, $\beta = 1$, $Re = 10^{-4}$ and $Ca = 10^4$. (a) evolution of $\theta(t)$ for the confinement parameter $\alpha = 1/2$ and $1/4$ for a vesicle with a reduced area $\gamma = 0.84$. (b) the stationary angle $\theta^* = \lim_{t\to+\infty} \theta(t)$ versus the reduced area γ for a vesicle in tank treading mode.

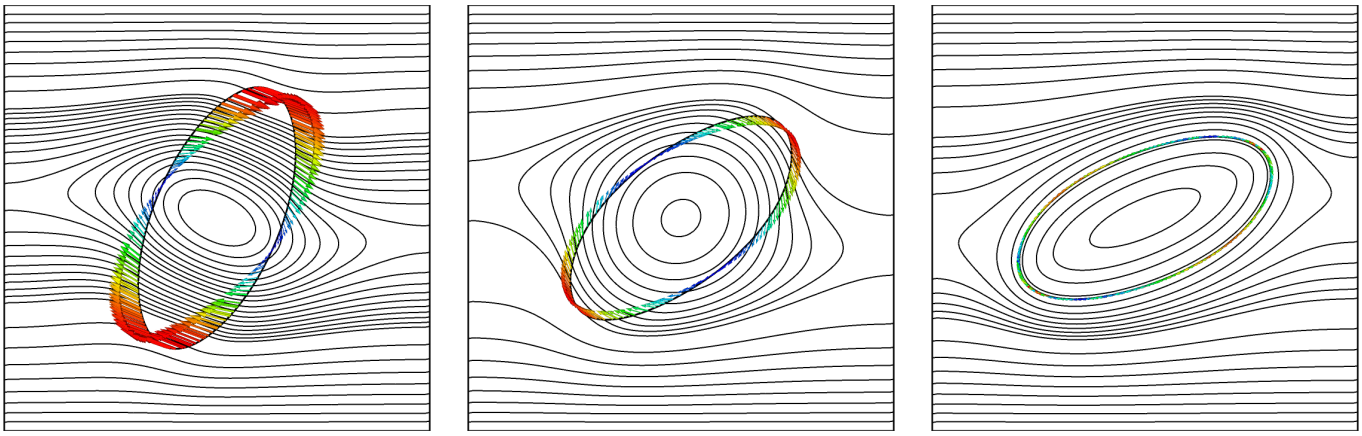

Figure 12: Tank-treading regime vs time for $\alpha = 1/2$ and $\gamma = 0.84$: streamlines lines and velocity field on the vesicle membrane $\partial\Omega$. Figures are, from left to right, at $t = k\Delta t$i, $k \in \{60, 120, 1000\}$ and $\Delta t = 2 \times 10^{-2}$.

about 10^{-3} Pa.s and ρ is about 10^3 kg.m^{-3}. For a mean velocity in the blood vessel about 1 m.s^{-1}, the Reynolds number $Re \approx 3$. In laboratory experiments, with experimental vesicles, R_0 is about 5×10^{-5} m while we can supervise vesicles using rapid cameras that can reach a velocity of about 0.1 m.s^{-1}. In that case, the Reynolds numbers $Re \approx 5$. In both cases, the inertia effect can no be neglected and the prediction of vesicle behaviors for this Reynolds numbers order. is of major importance; Moreover, we show in this paragraph, that for Reynolds number of this order of magnitude, the vesicle behavior will change dramatically for the simple shear flow.

Fig. 13 plots the evolution of the vesicle for $Re = 0.4$. Observe that the behavior, is dramatically different to the corresponding one for small Reynolds numbers, as on Fig. 4.b. Especially, deformations are more important when the inclination angle is close to $\pi/2$.

Above a critical value of the Reynolds number, the tumbling regime, as predicted by Keller and Skalak [21], disappears: a new tank-treading regime occurs and the vesicle keeps a constant angle. Figs. 14.a and 14.b plot the angle $\theta(t)$ for $\gamma = 0.82$: observe that the period T_p increases with Re until a critical Reynolds number between 3.5 and 4. For $Re > 4$, the angle $\theta(t)$ becomes constant: the vesicle switch from a tumbling regime to a tumbling one.

5 Conclusion

The new level method presented in this paper for the simulation of the vesicle dynamics exactly satisfies locally and at the discrete level both the inextensibility membrane condition and the volume conservation. We show that the proposed method, based on Lagrange multipliers, solves a lack of precision problem when dealing with the inextensibility constraints and the level set method. Moreover, an automatic adaptive method, used at each time step, enhance the prediction of the vesicle motion. With this procedure, we are able to accurately reproduce the change of regime, from tank-treading to tumbling, as observed when the viscosity ratio varies.

For the first time to your knowledge, we show the apparition of a new change of regime when the Reynolds number is below a critical value. Moreover, the critical Reynolds number of this order of magnitude for both red blood cells in arteries and vesicles used in laboratory experiments. In the future, new experiments on vesicle would be necessary to infirm or confirm your numerical predictions.

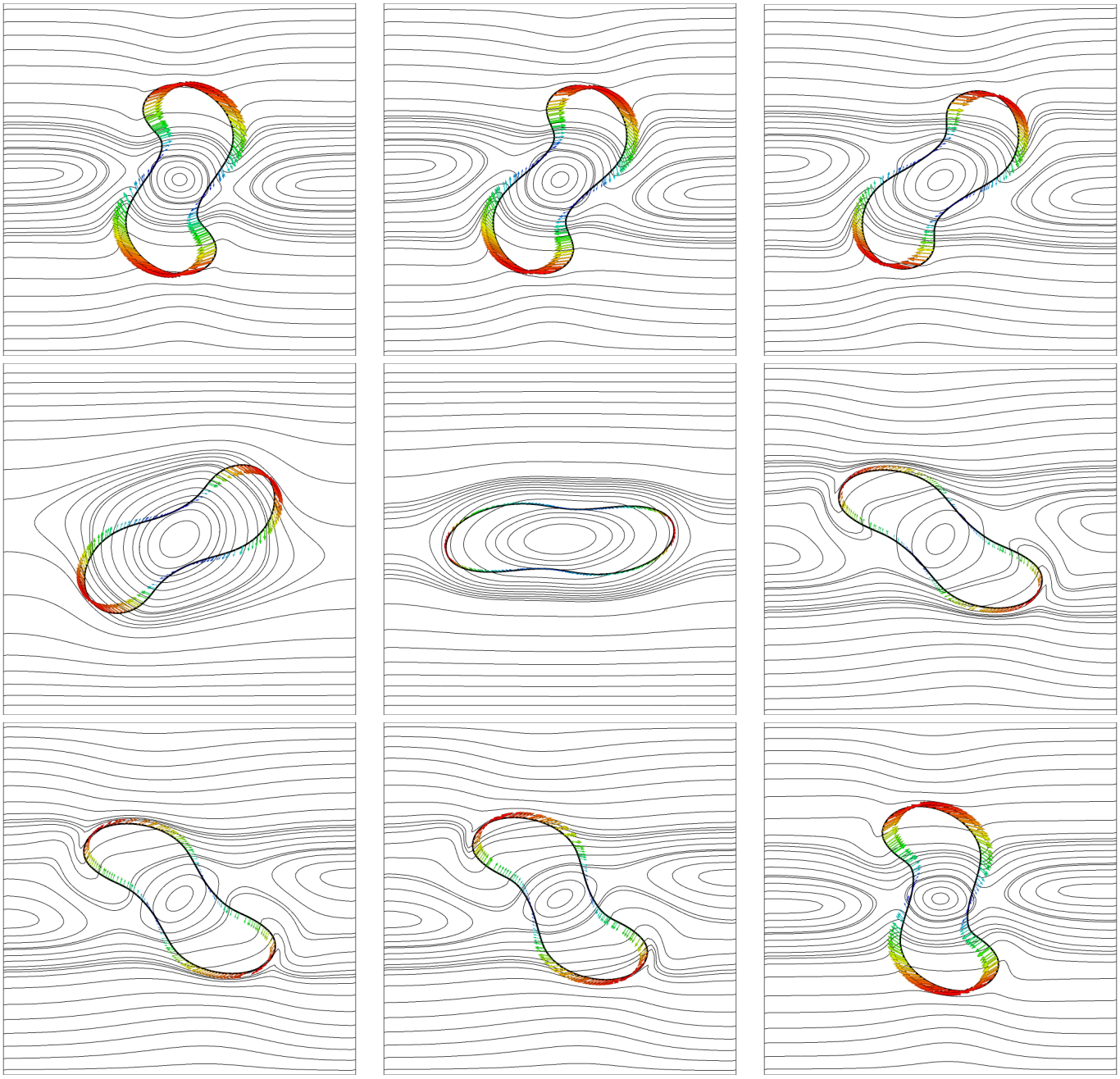

Figure 13: Inertia effects: streamlines lines and velocity field on the vesicle membrane for $\alpha = 1/2$, $\gamma = 0.62$, $\beta = 10$ and $Re = 0.4$. Figure are shown, from left to right and top to bottom, at $t = kT_p/24$, $k \in \{2, 4, 6, 8, 13, 18, 20, 22, 24\}$, where $T_p = 29.1$ is the tumbling period.

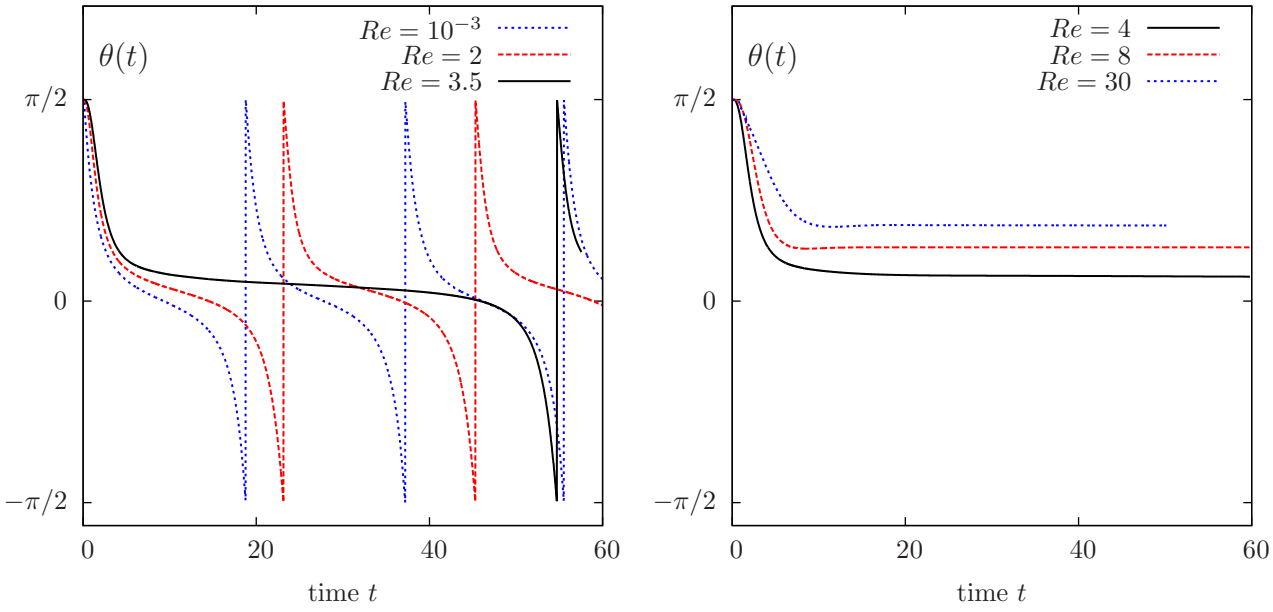

Figure 14: Inertia effect: influence of Re on the vesicle inclination $\theta(t)$, for $\gamma = 0.82$ regime: (a) tumbling regime when $Re \leq 3/5$; (b) tank-treading regime when $Re \geq 4$.

References

[1] R. A. Adams and J. J. F. Fournier. *Sobolev spaces*. Elsevier, second edition, 2003.

[2] S.M. Allen and J.W. Cahn. A microscopic theory for antiphase moundary motion and its application to antiphase domain coarsening. *Acta Metal.*, 27:1085–1095, 1979.

[3] G. Aubert and P. Kornprobst. *Mathematical problems in image processing. Partial differential equations and the calculus of variations*. Springer, second edition, 2006.

[4] T. Biben, K. Kassner, and C. Misbah. Phase-Field approach to three-dimensional vesicle dynamics. *Phys. Rev. E*, 72, 2005.

[5] T. Biben and C. Misbah. Tumbling of vesicles under shear flow within an advected-field approach. *Phys. Rev. E*, 67:031908, 2003.

[6] S. C. Brenner and L. R. Scott. *The mathematical theory of finite element methods*. Springer, third edition, 2008.

[7] F. Brezzi and M. Fortin. *Mixed and hybrid finite element methods*. Springer, 1991.

[8] C. Bui, V. Lleras, and O. Pantz. Dynamics of red blood cells in 2d. *ESAIM Proc.*, 28:182–194, 2009.

[9] P.B. Canham. The minimum energy of bending as a possible explanation of the biconcave shape of the human red blood cell. *J. Theor. Biol.*, 26:61–81, 1970.

[10] G.-H. Cottet, E. Maitre, and T. Milcent. Eulerian formulation and Level-Set models for incompressible fluid-structure interaction. *M2AN*, 42:471–492, 2008.

[11] Q. Du, C. Liu, R. Ryham, and X. Wang. Energetic variational approaches in modeling vesicle and fluid interactions. *Physica D*, 238:923–930, 2009.

[12] Q. Du, C. Liu, and X. Wang. A Phase Field approach in the numerical study of the elastic bending energy for vesicle membranes. *J. of Comput. Phys.*, 198:450–468, 2004.

[13] L. Formaggia and S. Perotto. New anisotropic *a priori* error estimates. *Numer. Math.*, 89:641–667, 2001.

[14] M. Fortin and R. Glowinski. *Augmented Lagrangian methods*. Elsevier, 1983.

[15] V. Girault and P. A. Raviart. *Finite element methods for the Navier-Stokes equations. Theory and algorithms*. Springer, 1986.

[16] G. H. Golub and C. F. Van Loan. *Matrix computations*. The John Hopkins University Press, Baltimore, MD, USA, third edition, 1996.

[17] F. Hecht. *BAMG: bidimensional anisotropic mesh generator*, 2006.

[18] W. Huang. Metric tensors for anisotropic mesh generation. *J. Comput. Phys.*, 204:633–665, 2005.

[19] W. Huang and X. Li. An anisotropic mesh adaptation method for the finite element solution of variational problems. *Finite Elements in Analysis and Design*, to appear:0, 2009.

[20] D. Jamet and C. Misbah. Toward a thermodynamically consistent picture of the phase-field model of vesicles: Curvature energy. *Phys. Rev. E*, 78:031902, 2008.

[21] S. Keller and R. Skalak. Motion of a tank-treading ellipsoidal particle in a shear flow. *J. Fluid Mech.*, 120:27–47, 1982.

[22] Y. Kim and M.-C. Lai. Simulating the dynamics of inextensible vesicles by the penalty immersed boundary method. *J. Comput. Phys.*, 229(12):4840–4853, 2010.

[23] T. Krüger, F. Varnik, and D. Raabe. Efficient and accurate simulations of deformable particles immersed in a fluid using a combined immersed boundary lattice Boltzmann finite element method. *Comput. Math. Appl.*, to appear, 2010.

[24] A. Laadhari, C. Misbah, and P. Saramito. On the equilibrium equation for a generalized biological membrane energy by using a shape optimization approach. *Physica D*, 239:1567–1572, 2010.

[25] A. Laadhari, P. Saramito, and C. Misbah. Improving the mass conservation of the Level Set method in a Finite Element context. *Comptes rendus mathématiques, Ser. I*, 348:535–540, 2010.

[26] E. Maitre, T. Milcent, G.-H. Cottet, A. Raoult, and Y. Usson. Applications of level set methods in computational biophysics. *Math. Comput. Model.*, 49(11–12):2161–2169, 2009.

[27] S. Osher and J.A. Sethian. Front propaging with curvature deppend speed: Agorithms based on Hamilton-Jacobi formulations. *J. Comput. Phys.*, 79(12), 1988.

[28] O. Pironneau. On the transport-diffusion algorithm and its applications to the Navier-Stokes equations. *Numerische Mathematik*, 38(3):309–332, 1982.

[29] C. Pozrikidis. Numerical simulation of the flow-induced deformation of red blood cells. *Annals of Biomedical Engineering*, 31:1194–1205, 2003.

[30] A. Rahimian, S. K. Veerapaneni, and G. Biros. Dynamic simulation of locally inextensible vesicles suspended in an arbitrary two-dimensional domain, a boundary integral method. *J. Comput. Phys.*, 229(18):6466–6484, 2010.

[31] S. A. Safran. *Statistical Thermodynamics of Surfaces, Interfaces and Membranes*. Frontier in Physics Vol 90. Addison-Wesley Publishing Company, Reading, MA, 1994.

[32] Pierre Saramito and Jocelyn Etienne. *Efficient scientific computing with Rheolef*. CNRS and LJK, 2011. `http://www-ljk.imag.fr/membres/Pierre.Saramito/rheolef/rheolef.pdf`.

[33] U. Seifert. Configurations of fluid membranes and vesicles. *Adv. Phys*, 46:13–137, 1997.

[34] V. Vitkova, G.Coupier, M.-A. Mader, B. Kaoui, C. Misbah, and T. Podgorski. Tumbling of viscous vesicles in a linear shear field near a wall. *Journal of optoelectronics and advanced materials*, 11:1218–1221, 2009.

[35] P. M. Vlahovska, T. Podgorski, and C. Misbah. Vesicles and red blood cells in flow: From individual dynamics to rheology. *Compte Rendus Physique*, 10:775–789, 2009.

[36] W.Helfrich. Elastic properties of lipid bilayers: theory and possible experiments. *Z. Naturforsch. Teil C*, 28:693–703, 1973.

[37] O.-Y. Zhong-can and W. Helfrich. Bending energy of vesicle membranes: general expressions for the first, second and third variation of the shape energy and applications to spheres and cylinders. *Phys. Rev. A*, 39(10):5280–5288, 1989.

A Remark on the spontaneous curvature

Let denote by V_0 the area and by A_0 the perimeter of the vesicle Ω. Using as a characteristic length the radius R_0 of the circle having the same perimeter as $\partial\Omega$, the relation between the Lagrangian $\mathscr{L}$ and its dimensionless counterpart $\widetilde{\mathscr{L}}$ writes:

$$\widetilde{\mathscr{L}}(\widetilde{\Omega};\widetilde{\lambda},\widetilde{p}) = \frac{2R_0}{k_c}\,\mathscr{L}(\Omega;\lambda,p) = \int_{\partial\widetilde{\Omega}} \widetilde{H}^2\,\mathrm{d}\widetilde{s} + \widetilde{\lambda}\left(\int_{\partial\widetilde{\Omega}} \mathrm{d}\widetilde{s} - \widetilde{A}_0\right) + \widetilde{p}\left(\int_{\widetilde{\Omega}} \mathrm{d}\widetilde{x} - \widetilde{V}_0\right).$$

where $\widetilde{\lambda} = \dfrac{2}{k_c}\,\lambda R_0^2$ and $\widetilde{p} = \dfrac{2}{k_c}\,pR_0^3$. denote the dimensionless Lagrange multipliers. Recall that the reduced area $\gamma = \dfrac{V_0}{\pi} \times \left(\dfrac{2\pi}{A_0}\right)^2 = \dfrac{V_0}{\pi R_0^2}$. Then, for the dimensionless problem, the volume and area express $\widetilde{V}_0 = \dfrac{V_0}{R_0^2} = \pi\,\gamma$ and $\widetilde{A}_0 = \dfrac{A_0}{R_0} = 2\pi$. As a consequence, the reduced area γ is the unique dimensionless number of this problem, that characterizes the stationary shape of the vesicle: others parameters, such as k_c, has no effects.

Let us turn to the effect of the spontaneous curvature $H_0 \geq 0$: The Lagrangian writes:

$$\mathscr{L}(\Omega;\lambda,p) = \frac{k_c}{2}\int_{\partial\Omega}(H-H_0)^2\,\mathrm{d}s + \lambda\left(\int_{\partial\Omega}\mathrm{d}s - A_0\right) + p\left(\int_{\Omega}\mathrm{d}x - V_0\right). \quad (30)$$

From $(H-H_0)^2 = H^2 - 2HH_0 + H_0^2$, notice first that the last H_0^2 term is constant and thus, has no effects in the minimization problem. The only term that depend upon H_0 is the second one, involving $H_0\int_{\partial\Omega} H\,\mathrm{d}s$. Using the general shape derivative analysis framework [24] with $f(H) = H$, we get, for any vector field $\mathbf{u}$:

$$\frac{\partial}{\partial\Omega}\left(\int_{\partial\Omega} H\,\mathrm{d}s\right)(\Omega).(\mathbf{u}) = \int_{\partial\Omega} 2K\,\mathbf{u}.\mathbf{n}\,\mathrm{d}s. \quad (31)$$

where K is the Gauss curvature of $\partial\Omega$. As $K = 0$ for two dimensional problems, the bidimensional vesicle equilibrium shape is independent of H_0 and depends only of the reduced area γ. The spontaneous curvature H_0 is only pertinent for three-dimensional problems.

B Remark on the redistanciation procedure

Let us consider the transport equation: $D_t\phi = \partial_t\phi + \mathbf{u}.\nabla\phi = 0$. Using the summation of repeated indices convention, we get: $\partial_i\phi\;\partial_i\partial_t\phi + \partial_i\phi\;\partial_i\left(u_j\partial_j\phi\right) = 0$ that writes also equivalently: $(1/2)\;\partial_t\left(|\nabla\phi|^2\right) + |\nabla\phi|^2(\mathbf{n}\otimes\mathbf{n}) : \mathbf{u} + \partial_i\phi.\partial_i\left(u_j\partial_j\phi\right)$. Remark that: $\partial_i\phi.\partial_i\left(u_j\partial_j\phi\right) = (1/2)\;u_j.\partial_j\left(\left(\partial_i\phi\right)^2\right) = (1/2)\;\mathbf{u}.\nabla\left(|\nabla\phi|^2\right) = |\nabla\phi|\mathbf{u}.\nabla(|\nabla\phi|)$.

Then, we obtain: $D_t(|\nabla\phi|) = |\nabla\phi|\ (\mathrm{div}_s\,\mathbf{u} - \mathrm{div}\,\mathbf{u})$. The density of the fluid is supposed to be constant, and the mass conservation leads to $\mathrm{div}\,\mathbf{u} = 0$. Moreover, in the context of vesicles, $\mathrm{div}_s\,\mathbf{u}$ since the membrane is supposed to be inextensible. Thus $D_t(|\nabla\phi|) = 0$. When $|\nabla\phi| = 1$ at $t = 0$, i.e. when ϕ is initially a distance function, this property is then preserved for all $t > 0$. When using the finite element approximation, we observe that this property is only approximately preserved, and thus, the redistancing procedure described in this paper is applied.

C Computation of the vesicle inclination

This appendix presents the computation of the angle θ of the shape Ω. Let (x_1, x_2) be the coordinate system for $\mathbb{R}^2$, containing the shape Ω and $\mathrm{d}x = \mathrm{d}x_1\mathrm{d}x_2$. The center of the vesicle is denoted by $(\bar{x}_1, \bar{x}_2)$, where $\bar{x}_1 = \left(\int_\Omega x_1 \mathrm{d}x\right)/\mathrm{meas}(\Omega)$ and $\bar{x}_2 = \left(\int_\Omega x_2 \mathrm{d}x\right)/\mathrm{meas}(\Omega)$. Let I be the inertia matrix of the vesicle relative to the vertical axis in $(\bar{x}_1, \bar{x}_2)$:

$$I_O = \begin{pmatrix} \int_\Omega (x_1 - \bar{x}_1)^2\,\mathrm{d}x & \int_\Omega (x_1 - \bar{x}_1)(x_2 - \bar{x}_1)\,\mathrm{d}x \\ \int_\Omega (x_1 - \bar{x}_1)(x_2 - \bar{x}_1)\,\mathrm{d}x & \int_\Omega (x_2 - \bar{x}_1)^2\,\mathrm{d}x \end{pmatrix}.$$

This symmetric matrix has two real eigenvalues and orthogonal eigenvectors. The inclination angle θ is defined as the angle between the eigenvector associated to the largest eigenvalue, and the x_1 axis.

Contents

List of Figures